REMOTE SENSING, MODELING, AND SYNTHESIS: ON THE DEVELOPMENT OF A GLOBAL OCEAN WIND/WAVE CLIMATOLOGY AND ITS APPLICATION TO SENSITIVE CLIMATE PARAMETERS

by

ERIK CHARLES BALDWIN STEVENS

B.S., University of Colorado at Boulder, 2009

A thesis submitted to the
Faculty of the Graduate School of the
University of Colorado in partial fulfillment
of the requirements for the degree of
Master of Science
Department of Aerospace Engineering Sciences
2010

This thesis for the Master of Science degree by

Erik Charles Baldwin Stevens

has been approved for the Department of

Aerospace Engineering Sciences

by

_____

Lakshmi H. Kantha

_____

Baylor Fox-Kemper

_____

William J. Emery

Date_____

The final copy of this thesis has been examined by the signatories, and we find that both the content and the form meet acceptable presentation standards of scholarly work in the above mentioned discipline.

Erik Charles Baldwin Stevens (M.S., Aerospace Engineering Sciences)

Remote Sensing, Modeling, and Synthesis: On the Development of a Global Ocean Wind/Wave Climatology and its Application to Sensitive Climate Parameters

Thesis directed by Professors Lakshmi Kantha and Baylor Fox-Kemper

In this study, data from TOPEX satellite altimetry is combined with ERA40 (ECMWF 40-year reanalysis) and non-data-assimilating WaveWatch3 model output to develop a comprehensive 2.5^{o}x2.5^{o} monthly global climatology of wind and wave properties useful in determining the global extent of Langmuir mixing. The climatology is forged from data covering the years 1994 - 2001. The variables mapped include: significant wave height, mean wave period, 10-meter atmospheric wind speed, skin friction velocity, wind direction, and wave direction. Further computation of surface Stokes drift and Langmuir number from these parameters exhibits sensitivity to data from the climatology, demonstrating its applicability and limitations for use as Langmuir turbulence forcing.

Agreement among the three data sources in the climatology is better than 90% for most basic wind/wave variables in the climatology, with wave period and wave direction showing the most disagreement. However, small disagreements in simple wave parameters lead to large discrepancies (approaching 50-100%) in estimates of Stokes drift and Langmuir number.

The average Langmuir number worldwide was found to be near 0.3 in regions of aligned wind and waves, but significantly less in trade wind regions. Scatter between the three sources in the average worldwide Langmuir number is 0.28 – 0.40, with the best-guess world average being ~0.35. Further study of the resulting

Langmuir number climatology reveals that the choice of Langmuir number definition has an impact on the statistics of the result by skewing the resulting Langmuir number histogram. Because of this, care should be taken to ensure proper use of means, medians, and standard deviations.

This study shows that comparing data assimilating and non-assimilating models illuminates the magnitude of missing model physics, and provides a check on the usefulness of model data versus empirical data. Context is gained by comparing multiple data sources rather than using just one.

This thesis is dedicated to my parents, Amy and Larry

ACKNOWLEDGEMENTS

I cannot express enough gratitude to my advisors, Baylor Fox-Kemper and Lakshmi Kantha for sharing their experience and opinions, and directing this research to completion. I am very grateful for Dr. Fox-Kemper's encouragement and dedication to ensuring my success in both this thesis and my research career in general. This work would not be as balanced or complete without the keen eye and insight of Dr. Kantha. Finally, I greatly appreciate the effort put in by Adrean Webb to generate data from the NOAA WaveWatch3 model, and that of Benjamin Hamlington and the Colorado Center for Astrodynamics Research for supplying satellite data.

This work was supported by NASA ROSES Physical Oceanography grant NNX09AF38G, a CIRES Innovative Research Project and a University of Colorado Innovative Seed Grant.

CONTENTS

TABLES

FIGURES

I. INTRODUCTION

1.1 Context

Attention in much of the scientific and political communities is increasingly focusing on climate modeling and the resulting predictions of Earth's near future. Recent drastic changes in the natural environment (Rosenzweig et al., 2007) have suddenly stepped out of the circles of the scientific community and signaled the urgency of climate change in the practical, everyday world. Consequently, scientific findings on the current state of the Earth system, such as the 2007 International Panel on Climate Change (IPCC) report are facing increasing importance and scrutiny.

The IPCC report represents a grand review of the recent work and research on the climate and its changes, summarizing the most influential predictions and results. The implications of the IPCC report are substantial to our economic and societal futures, and as a result, public attention and political agendas have finally begun to address these issues quite seriously. With this increased regard for climate modeling, demands for accuracy of the predictions made and the consequences of predictive error are becoming substantial.

The ability of a model to predict reality should depend on the extent to which it accounts for the initial conditions (i.e. empirical environmental data) and the accuracy to which it resolves all of the processes governing change (Sterl and Caires, 2005). Thus, to be fully correct in our predictions about the future, we

must include completely accurate measurements of the environment, and correctly simulate all of the processes that manipulate the present conditions into a future state. The current state of computer climate models is an approximation of this ideal representation. The models include many of the well-understood processes as governing equations and many of the hard to model processes as parameterizations. Still, there are likely many unknown contributors to global climate that are left out. One example of a process missing from climate models is explicit treatment of Langmuir turbulence and mixing – which is the motivation for the work herein. The available initial data and forcing is sufficient and *mostly* accurate, though spatial and temporal coverage is generally lacking over the open ocean. Still, there will always be much unknown about the Earth system as a whole, and there will always be pieces missing from our climate models.

1.2 Stokes Drift

In the absence of surface currents, the motion of a particle at the ocean surface is tied to the motion of surface gravity waves. As a wave propagates under the particle, the particle is thrust up and forward horizontally along the surface until the ridge of the wave is underneath. The particle then falls down and backward horizontally as the wave propagates away. In this way, the particle's path makes an elliptical orbit with the period of the wave. However, this orbit is not closed. The particle actually travels further in the direction of wave propagation than it falls backwards as the wave moves away. As a result, the ocean surface exhibits a mean velocity in the direction of the wave field, due only

to the motion of the waves themselves. This velocity is referred to as the Stokes drift (Kantha and Clayson, 2000).

Stokes drift is important because it acts as a source of energy to generate additional turbulence in the oceanic mixed layer (Kantha and Clayson, 2000). Stokes drift decays exponentially with depth, creating shear. This shear extracts energy from the wave field, converting it to turbulence. It is estimated that this energy extraction from the wave field is as significant worldwide as energy dissipation found in surf zones at the ocean edges (Kantha et al. 2009). Additionally, the vorticity created by Stokes drift at the ocean surface provides for the genesis of Langmuir mixing (Kantha and Clayson, 2000).

1.3 Langmuir Mixing

One phenomenon presently missing explicit treatment in global climate models is Langmuir mixing due to Langmuir cells and Langmuir turbulence (Sullivan, McWilliams & Moeng 97, Sullivan & McWilliams, 2010). Commonly named windrows, Langmuir cells are known to enhance vertical mixing in the upper mixed layer of the ocean wherever they exist (e.g., Plueddemann et al., 1996, D'Asaro & Dairiki, 1997). Because of this enhanced mixing they have an effect on sea surface temperature, near-surface stratification, and energy, momentum, and gas fluxes, which are key factors in worldwide climate.

Langmuir cells appear in long vortex pairs aligned parallel to the wind and wave directions (or between the two). The spacing between cells is usually 5-300 meters. Vertical velocities between the cells are quite high at 2-6 cm/s

downwelling and 1-2 cm/s upwelling. For this reason, Langmuir cells are capable of significant vertical transport of gases, momentum, turbulence, and energy in the ocean mixed layer (Kantha and Clayson, 2000). Langmuir turbulence is a more disorganized form of near surface overturning, with overturning cells elongated in roughly the wave and wind direction (Sullivan and McWilliams, 2010) and vertical kinetic energies that exceed the scaling from solid-wall boundary layers (D'Asaro and Dairiki, 1997) by a factor of 1.5-5.

There is ongoing debate on how strong, deep, and influential Langmuir cells are to sea surface temperature and other important processes, as well as the extent to which they occur in the world's complex and meagerly mapped oceans. They appear to generate and decay quickly and are therefore hard to study in the field (Kantha and Clayson, 2000). Climate models do not explicitly include any Langmuir cell physics, instead simply matching the depth of the mixed layer to available measurements. While this may be sufficient to map upper-ocean mixing in some areas, there are other regions, e.g. the Southern Ocean, where a persistent shallow bias exists in the modeled mixed layer depths. Ongoing work by Webb et al. (2010) is closely investigating how climate models react to the inclusion of Langmuir mixing, but there is still disagreement in the computation of turbulent Langmuir number, a parameter thought to be involved in controlling the strength of Langmuir mixing at any location (e.g., Harcourt & D'Asaro 2008). Though the principle of the Langmuir number (*La*), that the strength of Langmuir mixing is proportional to the ratio of surface Stokes drift velocity to wind friction velocity,

is agreed upon, the scaling of the relationship is still uncertain. Additionally, the exact response of Langmuir mixing to misalignment of the wind and waves is poorly understood. For this study, a common approximation for this response is used: *La* is proportional to the cosine of the angle between the wind and waves, as evidenced by the dot product in Eqs. 1 below.

The scaling of La can generally be thought of in three different forms. One of these forms, the Kantha number (after Lakshmi Kantha, who proposed it), provides a sound logical basis for the computation: that Kantha number increases as wave activity increases and scales precisely with the Stokes production term of energy. For this study, the Kantha number and the inverse-square of the Langmuir number (La^{-2}) (Eqs. 1) are presented side by side for comparison.

$$La = \left(\frac{|\boldsymbol{u}^*|^2}{\boldsymbol{U_S}\cdot\boldsymbol{u}^*}\right)^{\frac{1}{2}} \qquad La^{-2} = \frac{\boldsymbol{U_S}\cdot\boldsymbol{u}^*}{|\boldsymbol{u}^*|^2}$$

$$Ka = \left(\frac{(\boldsymbol{\tau}/\rho)\cdot\boldsymbol{U_s}}{\boldsymbol{u}^{*3}}\right)^{1/3} \rightarrow \left(\frac{|\boldsymbol{U_s}|}{\boldsymbol{u}*}\right)^{1/3} \tag{1}$$

…where $\boldsymbol{U}_s$ is Stokes drift and $\boldsymbol{u*}$ is ocean surface friction velocity due to wind.

The main uncertainties in Langmuir number computation involve knowledge of the global ocean wind and wave state. Computed from a few key variables (wave height, wave period, wind speed, and wind and wave directions), the Langmuir number is quite sensitive to small changes in wave height and period. Thus, large errors can easily result from inaccuracies in the current wind and wave datasets.

A key issue is uncovered by the inclusion of Langmuir number in climate models: the important end projections from climate models may depend greatly on sensitive reactions to the wind and ocean wave forcing. Small errors in the wind/wave climatology may therefore introduce large, unreal disturbances to the modeled climate. This is a manifestation of a principle that seems obvious: if we wish to clearly map and understand the Earth system as a whole, we must first understand its most basic pieces. A goal of this work is to quantify the likely values and uncertainty in different estimates of these variables, so that future climate model predictions of these variables can be checked for agreement with extant data.

1.4 Current Ocean Datasets

Satellite-retrieved wave data is a great resource because of its empirical nature and near global coverage. Satellite altimeters can directly and accurately measure wave height, and properties of the returned altimeter radar beam can indirectly give us information about the wind speed, wave period, and other important oceanographic parameters (see Gourrion et al., 2002, Vandemark et al., 1996, Gommenginger et al., 2003, etc.). Unfortunately, these indirectly measured data are based on empirical fits, and there is enough scatter around the fits to generate significant potential errors. Satellite altimetry is discussed in more detail in Section 2.1.1.

Additional ocean data can be retrieved from networks of floating instruments. These include ARGO floats, moored buoy arrays, and surface

drifters. There have also been several large-scale ship-based research campaigns to map the properties of the world's oceans. Though the ship data is thorough, its coverage in time and space is insufficient for creating a climatology of the average world ocean. Similar problems exist for moored buoy arrays due to their locations near continental shelves and shores, and non-continuous time coverage. ARGO floats may provide some of the data needed to create a climatology, and could be an important source of comparison data.

A model dataset, the EMCWF Reanalysis (ERA40), assimilates empirical wind and wave data to generate comprehensive global wind and wave fields for the past half-century. The primary focus of the ERA40 is the global atmospheric state, and the wave field is used to improve the air-sea momentum transfer (and also to estimate the wave field). Aside from the wave model, there is not a full ocean model in ERA40, thus it is not a true climate model. While certain aspects (wave height and wind speed, for example) of the climatology created from ERA40 are quite robust, others (wave period and direction) are still open to question. There is disagreement in these variables between ERA40 and other models, as well as satellite wave data. It should be noted that while satellite and buoy wave data are assimilated in ERA40, buoy data is sparse and the only satellite data assimilated is significant wave height (not period or other variables). There has been much work done to validate the ERA40 data (see Section2.1.2), and regions of error have been uncovered.

1.5 Thesis Overview

While considerable work has gone into comparing certain variables between the various wind and wave datasets available (see Caires et al., 2004, Bidlot et al., 2002, Hanson et al. 2009, Hwang et al. 1998, etc), no work has yet been done to fully quantify the differences between their methods and reconcile the disagreement between their results. There is a need for the models and observations to be combined into a comprehensive picture of the characteristic Earth wind and wave fields. A question remains: How can information from satellites, computer models, and in situ observations be accurately combined to represent this complex and dynamic truth?

This study sets out to answer this question. A new ocean wind/wave climatology (a multimodel ensemble average) is developed for the following variables: significant wave height (H_s), mean second-moment wave period (T_m), 10-meter wind speed and direction (U_{10}), surface friction velocity (u^*), and surface Stokes drift (U_s) magnitude and direction. It is hoped that this dataset will validate the accuracy of future parameterizations and models of natural wind and wave phenomena, leading to a better understanding of Earth's dynamic climate system and the role of remote sensing and modeling in climate science.

The usefulness of the new climatology is demonstrated by a case study in which the climatology data is used to compute the highly sensitive inverse-square Langmuir (La^{-2}) and Kantha (Ka) numbers. This new Langmuir mixing

climatology will answer the question: how strong and prevalent is Langmuir mixing worldwide?

II. METHODOLOGY

2.1 Data Sources

Three overlapping sources were used in this study to compile the wind/wave climatologies so as to reconcile any differences and cover any shortcomings in the data. The three data sources are TOPEX satellite altimetry, the European Center for Medium-Range Weather Forecasts' (ECMWF) ocean-atmosphere model reanalysis (ERA40), and the NOAA WaveWatch3 (WW3) model. They were chosen because they represent a subset of three independent wave data sources overlapping globally, from which the study period was chosen to be from 1994 to 2001. While there are other satellite altimeters that could have been used for this study, TOPEX provides the longest contiguous satellite record from one instrument and has been highly validated and scrutinized in the literature; its properties and retrievals have been well-studied. An overview of each data source is found in Table II-1.

Table II-1: Summary of data

Source	Strengths	Weaknesses	Spatial Coverage	Temporal Coverage
TOPEX	H_s (4cm)	Everything else (mostly)	~Global, (66°N to 66°S lat.)	~10 day repeat period, 1993 – 2001
ERA40	H_s, U_{10}	Data assimilation periods	Global	Every 6 hours, 1957 – 2002
WW3	2D spectrum Stokes drift	Forcing field is arbitrary, no assimilation	Global	Every 3 hours, as desired

2.1.1 TOPEX Altimetry

TOPEX altimetry consists of Ku-band radar altimeter data, retrieved remotely aboard a satellite orbiting at 1336km above the ocean surface. The altimeter data is collected in a pushbroom architecture, with passes inclined at 66^{o} to the equator. By measuring once per second, it provides data with roughly 7km resolution. The repeat period for any given point is roughly ten days (Hwang et al., 1998).

TOPEX data is not truly global in coverage since the satellite orbit inclination limits data coverage to 66^{o}N to 66^{o}S. The lack of coverage poleward of 66^{o} latitude is inconsequential for this study, as sea ice or landmass dominates much of this area for much of the year. Based on current literature, the bulk of current interest in wind-wave interaction is focused on the ice-free open ocean – the area to which this study pertains.

Wave height (H_s) is the characteristic oceanographic parameter retrieved by TOPEX. The instrument sends out 4,000 pulses per second, and averages these data into one-second measurements. Wave height is then determined from the average radar return waveform variance, with a nominal accuracy of 4-5cm (Chelton et al., 1989).

TOPEX also returns the normalized radar cross section for each measurement, and the empirical model of Gourrion et al. (2002) is used to covert this into 10-meter wind speed (U_{10}). The U_{10} data was calculated and furnished by

Benjamin Hamlington at the Colorado Center for Astrodynamics Research (CCAR) in Boulder, CO.

Given u_{10}, the models of Vandemark et al. (1996) and Gommenginger et al. (2003) are used to find the friction velocity (u^*) and mean wave period (T_m) (both also furnished by Benjamin Hamlington) respectively, as follows:

For $U_{10} < 2.4$m/s:

$$Cd10 = [(\frac{1}{\kappa}) \ln(Cd_{10}{}^{1/2} U_{10} \frac{10}{\upsilon}) + 5.5]^{-2}$$

For $U_{10} > 2.4$m/s:

$$Cd10 = [(\frac{1}{\kappa}) \ln(Cd_{10}{}^{1/2} U_{10} \frac{10}{\upsilon}) + 5.5]^{-2} \quad (2)$$

Then,

$$u^* = Cd_{10}{}^{1/2} U_{10} \quad (3)$$

And,

$$T_m = -0.895 + 2.545P \quad (4)$$

Where,

$$P = (\sigma_0 H_s{}^2)^{0.25} \quad (5)$$

Gourrion et al. (2002) report that altimeter backscatter is proportional to both wind speed and sea state, and thus sea state biases are corrected for in the U_{10} model. The result is a wind-independent bias of less than 0.3m/s in TOPEX u_{10} as compared to buoys, models, and satellite scatterometers.

Vandemark et al. (1996) found their model (Eqs. 2 and 3) to produce a roughly 0.02m/s bias in u^*, with a root-mean square-error (RMSE) near 0.038m/s

versus in situ (ship-derived) observations. They also demonstrated that higher accuracies can be achieved by directly correlating u^* to radar cross section (σ_o), rather than deriving U_{10} from σ_o and then u^* from U_{10}. However, a well-tested model as such was not available for this study.

The T_m relationship used here (Eq. 4) is derived from regression against buoy wave period data, with a reported RMSE of roughly 0.98s (about 7%) (Gommenginger et al., 2003). An extensive study by Caires et al. (2005) shows that the Gommenginger T_m model is biased in swell-dominated seas and for wind speeds less than 10m/s. With these points removed, they found the TOPEX-ERA40 RMSE to be 0.77s.

2.1.2 ERA40 Reanalysis

The ERA40 dataset, completed in 2004, is a 45-year reanalysis run of the European Center for Medium-Range Weather Forecasts (ECMWF) meteorological (atmosphere) model, coupled to a 3rd-Generation WAM wave model (Komen et al., 1994). The coupling consists of the 10-meter wind speed, U_{10}, from the atmosphere model being passed to the wave model every four time steps (hourly). The WAM 3.0 wave model used in ERA40 uses energy balance equations to derive the full wave spectrum without any restriction of its spectral shape. Wave parameters (H_s, T_m, etc.) are accurately calculated by integrating this full wave spectrum, and then the wave spectrum itself is deleted (Sterl and Caires, 2005). Since the spectrum is not saved, some additional wave parameters (e.g. Stokes Drift) can not be directly calculated, but must be approximated from the

data available and assumptions about the average wave spectrum. This disadvantage of the ERA40 data limits its usefulness for estimating complex and interesting wave properties and effects.

The coupled wind-wave model was run to generate the atmosphere and sea state for 1957 to 2002, using a 3DVAR technique to assimilate all available empirical atmospheric data, as well as ERS-1 and ERS-2 satellite altimeter H_s data. This assimilation essentially pushes the model toward the measured reality. Thus the model is constantly tuned to match wind and wave data throughout the period, and is not expected to deviate significantly from this input. By providing complete gridded data for the majority of atmosphere-ocean interaction, the ERA40 reanalysis fills obvious and problematic data gaps and discontinuities in the wind and wave measurement record (Sterl and Caires, 2005).

The data coverage advantage outweighs the potential errors contributed by the assumptions and simplified physics that go into models, but to assume that the model data is essentially correct simply because some of its parameters are tuned to real data would be incorrect. Instead, I treat the ERA40 model dataset as representing a reality parallel to what was observed from 1957 to 2002. These two realities likely have many similarities and some potential differences.

It is expected that the model output of H_s is essentially the same as the observed ERS satellite H_s data, which were assimilated, but only for the period of assimilation. In fact, distinct differences in the ERA40 data from different data assimilation periods are clear. Figure II-1 shows monthly mean worldwide H_s for

the entire ERA40 period. According to Sterl and Caires (2005) there are four distinct data assimilation periods:

Period 1 (September 1957 to November 1991): No satellite H_s information is assimilated during this period. Though the average wave field compares well with observations, ERA-40 generally underestimates high wave heights and overestimates low ones.

Period 2 (December 1991 to May 1993): Faulty ERS-1 H_s data are assimilated, and ERA40 H_s values between 1-3m are overestimated compared to buoy data. H_s data quality for heights above 3m is similar to that in period 1.

Period 3 (January 1994 to May 1996): Assimilated ERS-1 H_s data are no longer known to be faulty, but a known calibration correction is not applied to H_s since it creates a positive bias in the T_m field.

Period 4 (June1996 to December 2002): Assimilation of calibrated ERS-2 H_s data. ERA40 still generally underestimates high wave heights, and slightly overestimates low wave heights.

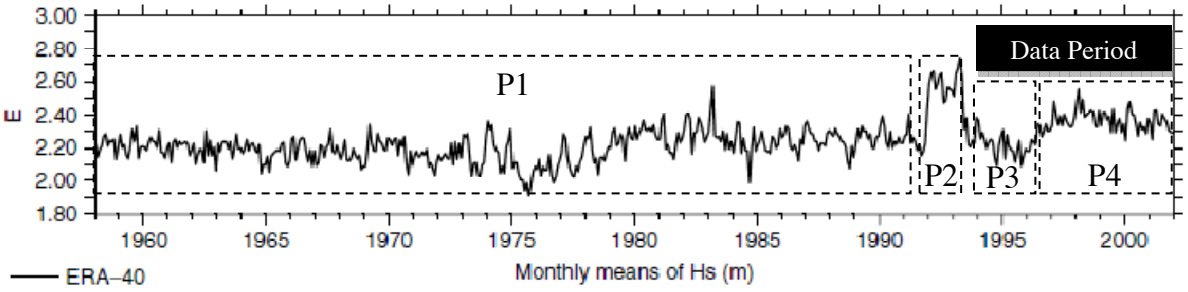

Figure II-1: ERA40 global mean wave height from 1958-2001. Data assimilation periods 1-4 are marked by dashed boxes, with this study's data period shown by the solid black box. Graph from Sterl and Caires (2005).

Since TOPEX data are available only from 1993-2001, ERA40 data before this period were not considered in this study. Additionally, the obvious discrepancy of ERA40 data during period 2 prior to 1994 was reason to narrow the time window for this study to 1994-2001. This eight-year period provides good data from both TOPEX and ERA40.

While the period 1 ERA40 data is not considered in this study, it is important to note that H_s data from this period matches buoy observations closely. Though this lends credence to the model, recall that buoys are only sparsely located, and their positions near populated shores and continental shelves may present potential biases compared to measurements of the global ocean as a whole. For example, there are no moored buoys in the stormy southern ocean where average H_s is the highest in the world.

Finally, the abrupt jump in H_s data seen during period 2 (Figure II-1) shows the drastic effect data assimilation has on the model. Because of this, measurement errors in the assimilated data are expected to translate well into

errors in the model output. The model is really only as good as the data going into it.

2.1.3 NOAA Wave Watch 3

WW3 is a 3rd-generation operational wave model with various improvements over WAM 3.0. A recent review (Cavaleri et al, 2007) found WW3 to be the most accurate model in use at the time. The underlying structure of WW3 uses different governing equations, numerical methods, physical parameterizations, and a unique architecture from WAM 3.0 (WAVEWATCH III Model, 2009). Because of this, it provides a completely independent source from ERA40 wave data and a third dataset to which wave comparisons can be made. The main advantage of WW3 over available ERA40 data is that the directional wave spectrum data are available for direct calculation of uncommon wave parameters (such as Stokes drift). Otherwise, wave parameters are calculated by integrating the 2D wave spectrum as in ERA40.

The main assumption in the WW3 governing equations is that water depth, current, and wave field vary on time and space scales much larger than the scales of individual waves. This should be generally correct on the global scale, and verification comes in the form comparisons to buoys and other models.

Hanson et al. (2009) showed WW3 to outperform WAM 3.0 in the Pacific Ocean based on comparison to seven buoys and nine different performance metrics. These metrics quantified the errors in wave height, period, and direction as derived from the wave spectrum under equal forcing.

Further validation of WW3 comes from Tolman (2002), who found WW3 errors to be generally less than WAM 3.0 as compared to both buoy and ERS-1 altimeter data, especially in tropical regions and in local areas of extreme wave heights (though poorer performance was found in some high-latitude regions). RMS errors for WW3 were found to be typically 15% for local H_s.

For this study, WW3 was run by Adrean Webb from the University of Colorado, Applied Math department. The model was run on the Bluefire super computer at the National Center for Atmospheric Research (NCAR) with the assistance of NCAR modeling experts. The wind model chosen to force the wave model (chosen by Adrean Webb to suit the needs of another project) was version 2.0 of the Common Ocean-Ice Reference Experiments (CORE 2.0) forcing (Large and Yeager, 2008). CORE 2.0 is a slightly different wind product than that used to force the WAM 3.0 wave model in ERA40, and a slightly different wave field is expected as a result. Both wind products are well accepted for forcing ocean models, so using the two fields gives a sense of the uncertainty among accepted wind products.

It is assumed for this study that the wind field over the ocean is generally well resolved in these models, since accurate and validated wind data of global coverage is available from satellite scatterometer missions. In other words, there is much more uncertainty about the wave field across the world's oceans than of the wind field that is forcing these waves. With this assumption, the differences between the resulting WW3 and ERA40 wave fields should predominantly be due

to differences in the physics and dynamics of the models themselves, and much less due to differences in wind forcing, although the differences in 10-meter wind speed and direction are briefly discussed herein.

2.2 Data Reduction

When comparing unique data sources, collocation in time and space is an inevitable problem. The very large amount of data involved here further complicated the preprocessing needed to make apples-to-apples comparisons. Regridding and logistical manipulation of the source data occupied the bulk of the time spent preparing this project, often requiring switching machines or techniques due to crashes, bugs, or resource overuse, sometimes several days into the running of a script. This study could have been completed twice in the same amount of time had everything worked properly the first time, but mistakes and unexpected crashes are the reality of working with copious amounts of data. One goal that has arisen as a result of this project is that the data I have taken the time to preprocess is available for research use. In this way, perhaps much more science can be achieved beyond what is already investigated here.

For this study, the final grid was chosen to match that of the standard ERA40 atmospheric data grid: 2.5^{o}x2.5^{o} and 6-hourly. To do this, WW3 data, which came originally in 3-hourly chunks, was decimated (every other timestep used) to match the temporal spacing of ERA40. After this, linear interpolation was used to regrid the data from a 1.25^{o}x1^{o} grid to the 2.5^{o}x2.5^{o} grid of ERA40. The WW3 fields are generally smooth over a distance of roughly 2 grid points, so

this interpolation is not expected to cause significant error, but it simplifies the comparison of the models.

The TOPEX data swaths were gridded by binning the measurements by the 6-hourly periods in ERA40. For each bin, the median of every TOPEX data point within a 2.5^{o}x2.5^{o} grid cell provided the data value for the center of that cell. Medians were taken to decrease sensitivity to outliers, as the TOPEX data is noisier than the model output from ERA40 and WW3. Figure II-2 shows the varying resolutions of each data source before gridding.

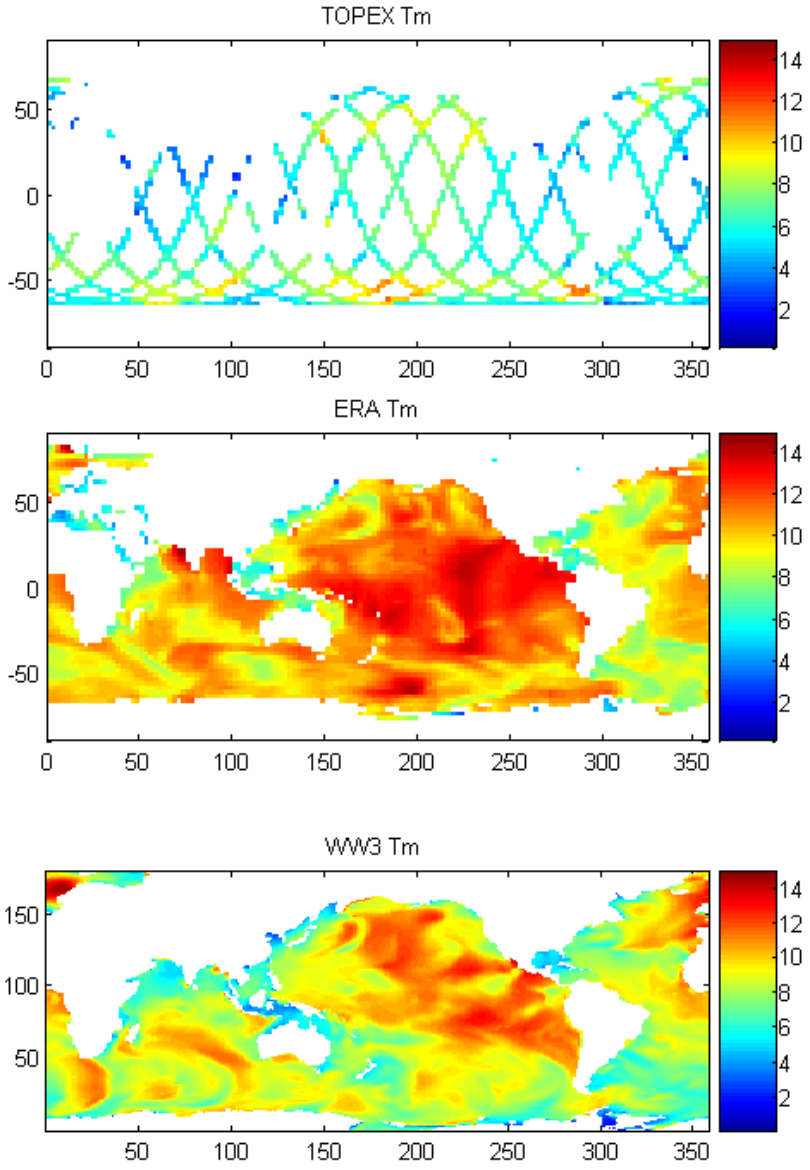

Figure II-2: Mean wave period (s) from each data source for February 8th, 1993. Note that this day falls within period 2 of the ERA40data history (see Section 2.1.2).

Once each available variable from each data source was gridded, the 6-hourly data was then temporally averaged (medians) for each month from 1994-2001. These monthly climatology data (presented seasonally in Appendix A) were used to calculate any secondary variables such as Stokes drift and Langmuir

number. Finally, the monthly data were binned and averaged (again, medians) to create the final fields presented here.

The choice of medians vs. means has a significant effect on the results of the TOPEX data because of general noisiness, especially in certain regions. These regions are discussed in more detail in Section 4.3. The mean - median difference (Figure II-3) shows these areas where noise skews the data distribution, causing inflated means. As the TOPEX wave period inversion is purely empirical, rather than being based on solid physical ground as are the significant wave height formulae, such outliers are perhaps not unexpected.

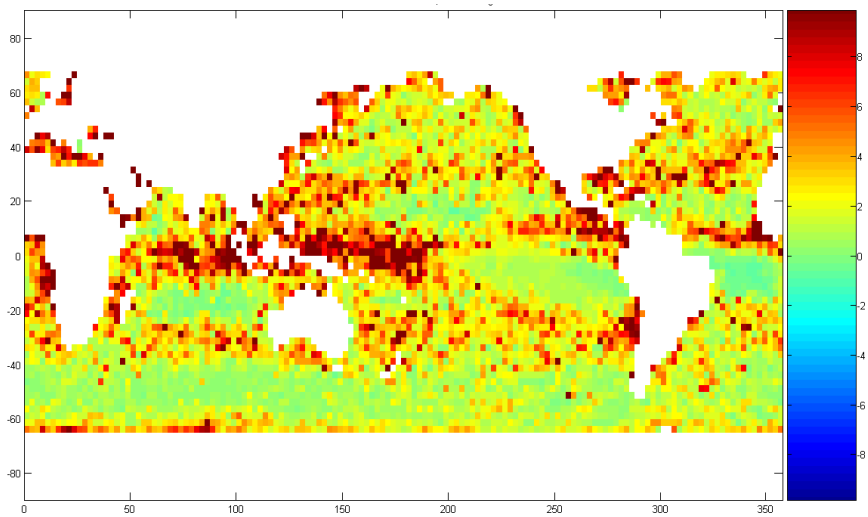

Figure II-3: TOPEX mean - median inverse-square Langmuir number for 1993. Colorscale goes from -10 to 10.

2.3 Calculation of Stokes Drift

In wave models, assuming all waves travel in the same direction, Stokes drift can be found by integrating the complete wave spectrum as seen in Eq. 6

(McWilliams and Restrepo, 1999). This method is implemented in our run of WW3, and yields results accurate to the wave field generated in the model.

$$\left|u_{s\_mr}\right| = \frac{2}{g}\int_0^\infty S_\omega(\omega)\omega^3 e^{2\omega^2 z/g}\,d\omega \qquad (6)$$

In ERA40, however, the wave spectrum was not available, so direct calculation of Stokes drift was impossible. TOPEX cannot measure the wave spectrum at all. Consequently Stokes drift must be approximated in both ERA40 and TOPEX. The Stokes drift in WW3, on the other hand, is calculated directly from the wave spectrum using Eq. 6. The approximation used here assumes a monochromatic wave spectrum formula with an empirical correction factor based on WW3 spectral calculations of Stokes drift. This approximation is expected to have an error less than the disagreement between WW3 and ERA40, so it is close enough for use here. The Stokes drift calculation for monochromatic waves is found in Eq. 7.

$$\left|U_{s\_approx}\right| = \frac{\alpha\pi^3 {H_s}^2}{g{T_m}^3} \qquad (7)$$

Here, α is an empirical parameter that is treated as a constant. It was estimated using WW3 data algebraically by setting the full-spectrum Stokes drift calculation (Eq. 6) equal to the approximation (Eq. 7) and solving for α. The result, α = 1.7088, provides a good approximation (around 0-15% error, best in stormy regions), as seen in Figure II-4.

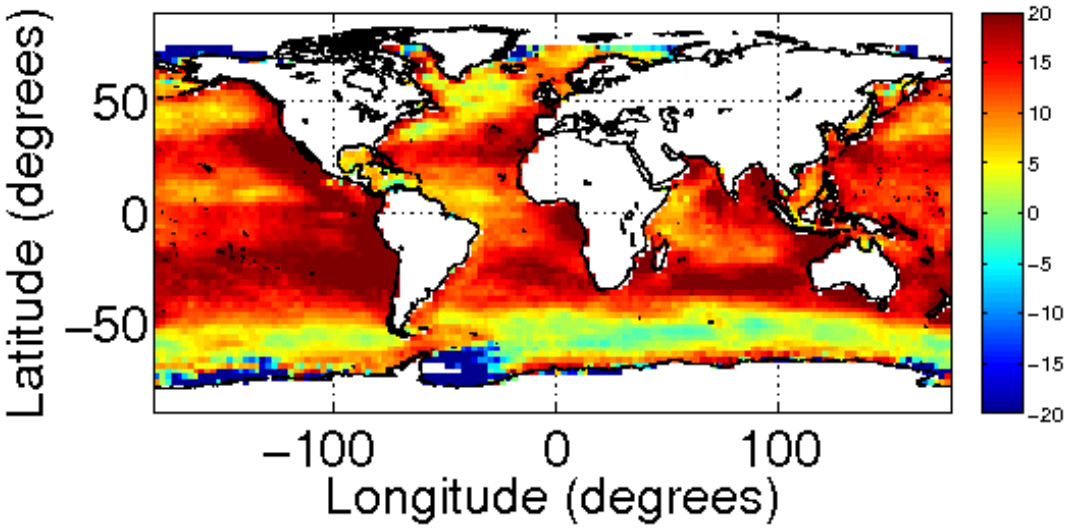

Figure II-4: Average percent difference U_{smr} - $U_{sapprox}$ from WW3

It is clear that α is not truly constant, and it may even be a function of wave age or wind speed. However, a function for α does not yet exist at the time of this research. Adrean Webb is currently exploring the behavior of α, and his results will be used in future calculations of Stokes drift.

There is implicit error in the TOPEX and ERA40 Stokes drift and Langmuir number in areas where α deviates from the constant value used here. It should be noted that these errors may approach 20% in the specific regions shown in Figure II-4.

2.4 Multimodel Ensemble Average

General confusion tends to come out of the disagreement in the wind/wave data scrutinized here between TOPEX, ERA40, and WW3. Reading the documentation and literature pertaining to each data source, one finds claims that

each source is the better than the others, and vast amounts of validation to prove it. While this seems contradictory, there are some general themes that can be pulled out of the literature to help sort the data. My attempt at this is presented in this study parallel to the three sources as a multimodel ensemble (MME).

TOPEX wave period, for example, can reasonably be dismissed as inaccurate for this study due to the reasons why it is regionally and climatologically biased, stated in Section 2.1.1. This leaves us with only the buoy-based validation studies completed so far (Caires et al., 2004, Bidlot et al., 2002, Hanson et al. 2009, Hwang et al. 1998, etc). The gist of such studies is that both WW3 and ERA40 are accurate in wave period to an equal degree, albeit with different wind forcing for WW3 than that used here. Because of this, I will treat wave period from both sources with equal weight, averaging them together to compress the scatter into one wave period field.

Since TOPEX does not measure wind or wave direction, it cannot be used to validate ERA40 or WW3 in these parameters. Interestingly, ERA40 and WW3 have slightly different wave direction fields (as will be seen in Section 3.1), even though their wind direction fields are nearly identical. This unintuitive result must stem from the large differences in model architectures and assumptions. To sort out whether one solution may be better than the other, I am relying on two things: 1) Both the literature and general community in oceanography lean towards WW3 as being superior in the accuracy of its wave field. 2) The WW3 model produces wind and waves that are aligned more often than in ERA40 (This will be shown in

Section 3.1, Figure III-7), a concept that is consistent with the general theory of wave production by wind. For these reasons, I consider the WW3 wave direction field to be the most correct available, and use solely it for wave direction in my multimodel ensemble climatology.

All other variables considered here are agreed upon closely enough that averaging them has little consequence, and is intuitive since they all represent the current limits of accuracy.

Another consideration is that the run of WW3 used here is essentially in another class of wave models from ERA40 because it does not assimilate any data. A consequence is that the two models may be outputting different views of the same truth. If this is the case, averaging them together is not necessarily the most correct way to estimate the true wave field. However, the logic behind the models is the same: to accurately model the true wave field. Each model does this to a different degree of accuracy, and neither can necessarily be proven as more correct based on the analyses here, so I weight them both equally for this study.

To summarize, the multimodel ensemble (MME) calculated for this study is composed of:

- Significant wave height: average of TOPEX, ERA40, and WW3
- Mean wave period: average of ERA40 and WW3
- Wind and wave directions: WW3
- Friction velocity: average of TOPEX, ERA40, and WW3

MME Stokes drift, Langmuir, and Kantha numbers are calculated from the MME variables outlined above. To decrease data-size, the wind and wave fields were averaged into monthly means before finding the Stokes drift and Langmuir fields. A preferred method would involve finding the Langmuir and Stokes drift fields before taking the averages. However, this was not feasible for this study due to data size, availability, and consistency constraints.

III. RESULTS

Climatologies resulting from each data source are shown below. They are presented in two ways: zonal averages and color-filled 2D contour fields. In most cases, zonal averages are sufficient to show the majority of worldwide variability and consistency with well-known global climate patterns such as wind belts. That is, often the data are banded in zonal stripes. A complete view of the data by season is found in Appendix A. Detailed discussion of the climatology will follow in Section IV.

For some lesser-known variables, I present the full two dimensional contour field of the world's oceans in addition to zonal averages, so as to fully introduce spatial patterns and extent. For those variables of which two-dimensional contour plots are not presented in this section, these data are found in Appendix A.

For the zonal average plots, the blue line shows data from TOPEX, red from ERA40, black from WW3, and green represents the multimodel ensemble developed for this study (Figure III-1). The green MME line is only included in zonal plots in which there is significant disagreement. For all other zonal plots, the MME can be assumed to follow the average of the TOPEX, ERA40, and WW3.

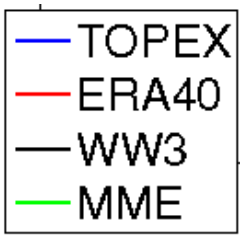

Figure III-1: Legend for climatology

3.1 Primary Wind/Wave Variables and their Climatologies

The first variables shown here are fundamental primary properties from which other wind-wave parameters are calculated. This group includes the most basic factors from which the wind and wave fields are measured or described: significant wave height (H_s), second-moment mean wave period (T_{m2}), ten-meter wind speed (U_{10}), wind direction (WD), mean wave direction (MWD), and the cosine of the angle between the wind and wave directions – $cos(\theta)$.

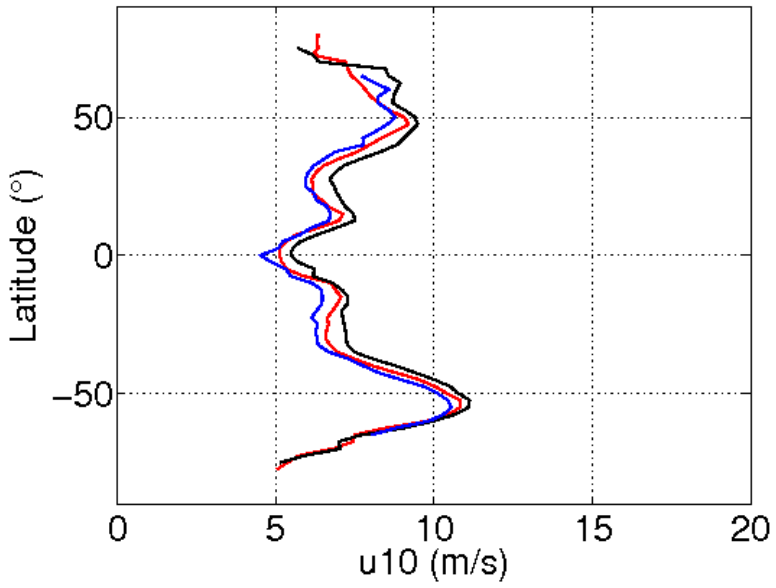

Figure III-2: Global zonal average of ten-meter wind speed from TOPEX (blue), ERA40 (red), and WW3 (black)

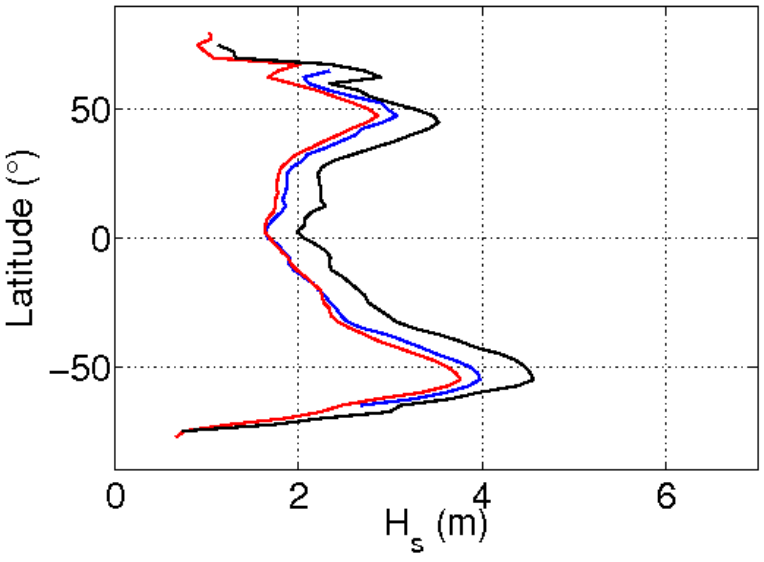

Figure III-3: Global zonal average of significant wave height from TOPEX (blue), ERA40 (red), and WW3 (black)

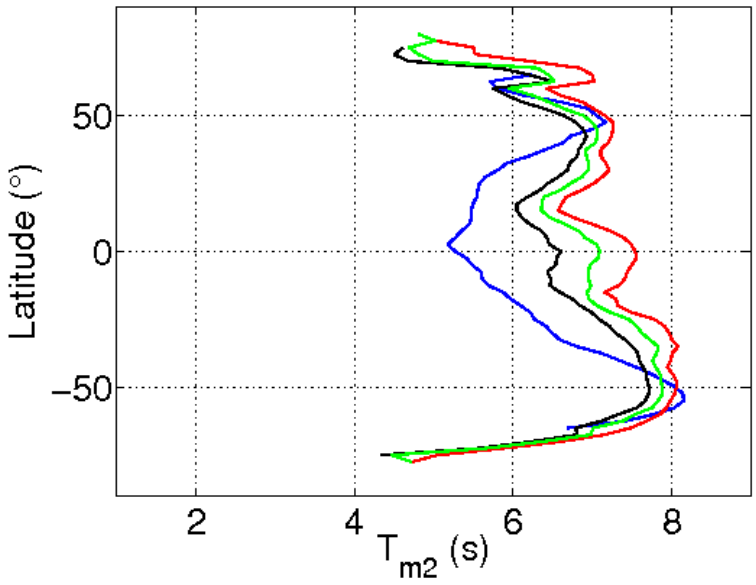

Figure III-4: Global zonal average of second-moment mean wave period from TOPEX (blue), ERA40 (red), WW3 (black), and MME (green)

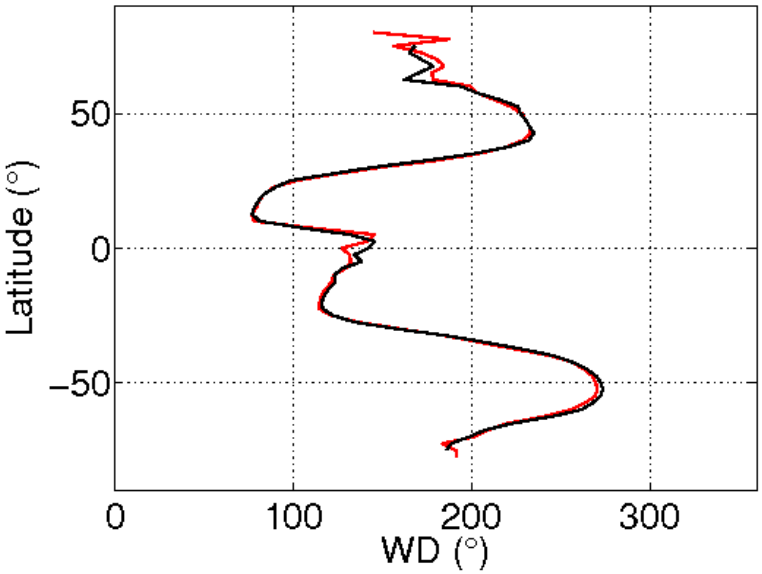

Figure III-5: Global zonal average of wind direction from ERA40 (red) and WW3 (black)

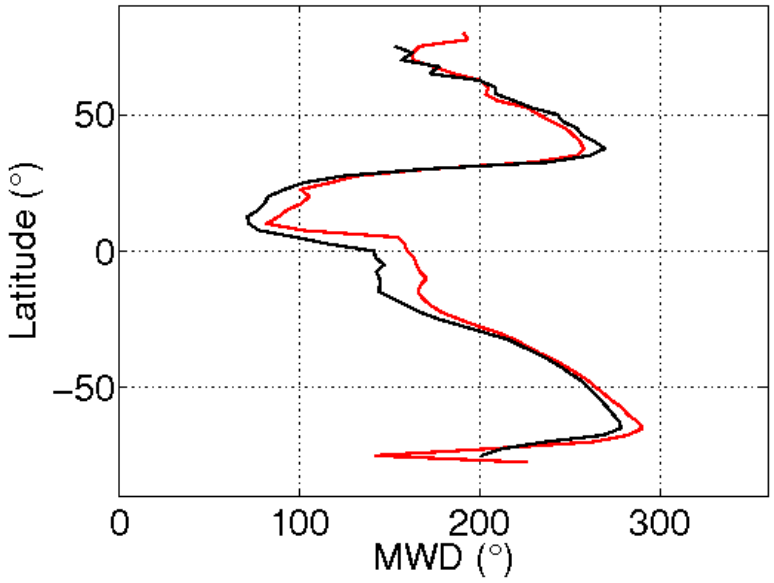

Figure III-6: Global zonal average of mean wave direction from ERA40 (red) and WW3 (black)

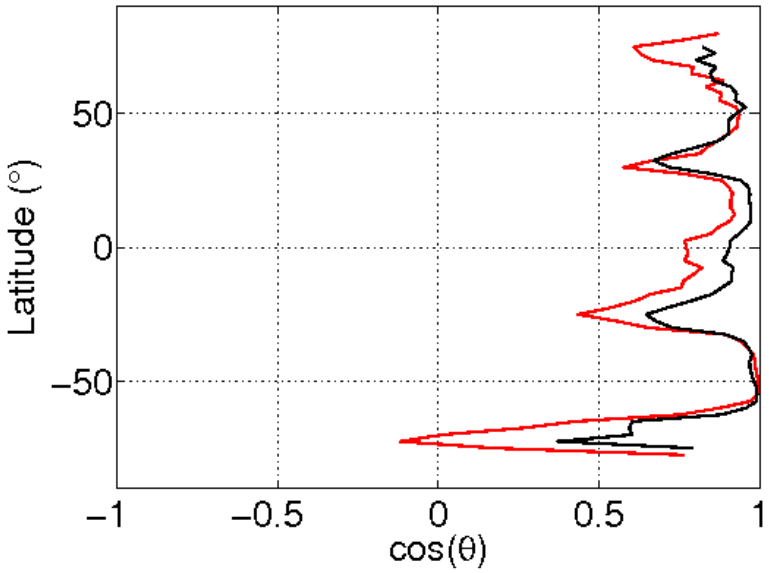

Figure III-7: Global zonal average of Cos(θ) from ERA40 (red) and WW3 (black)

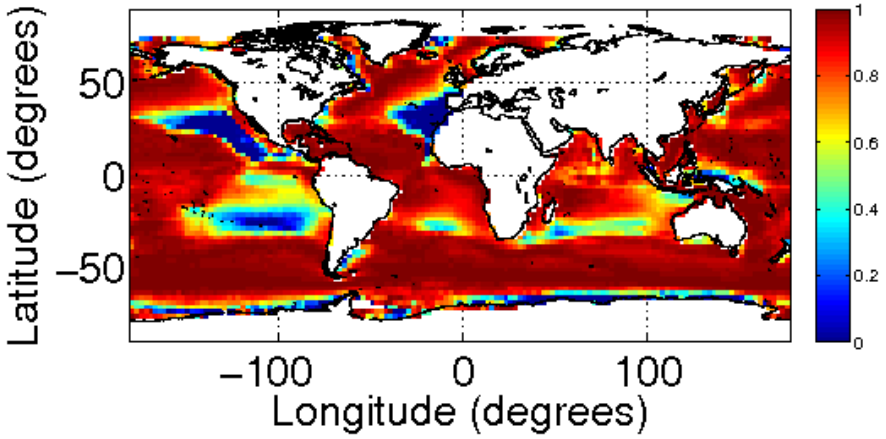

Figure III-8: Global average cos(θ) from WW3.

3.2 Secondary Variables

Next, I present climatologies of the derived wind/wave parameters that are calculated directly from the variables shown in Sections 3.1 using Eqs. 1, 6, and 7. They are surface friction velocity (u^*), surface stokes drift (U_s), inverse-square turbulent Langmuir number (La^{-2}), and Kantha number (Ka).

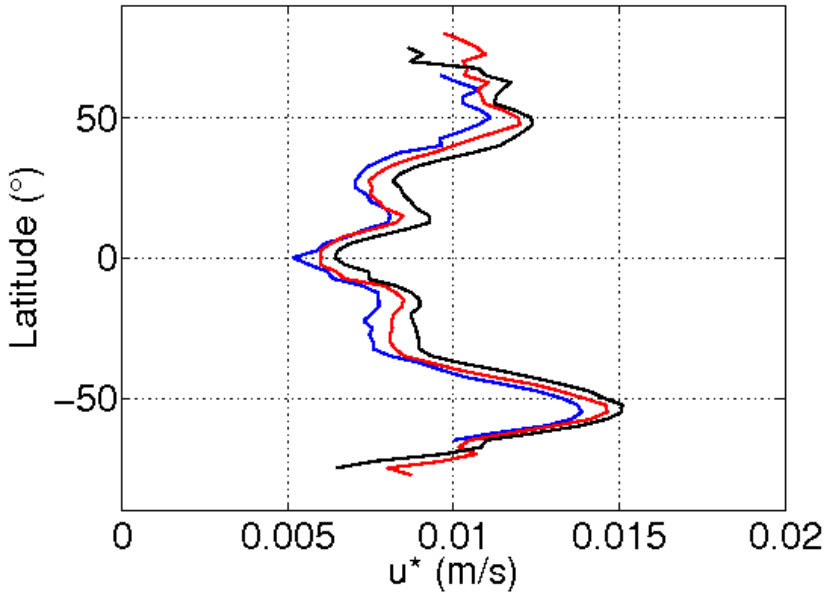

Figure III-9: Surface friction velocity from TOPEX (blue), ERA40 (red), and WW3 (black)

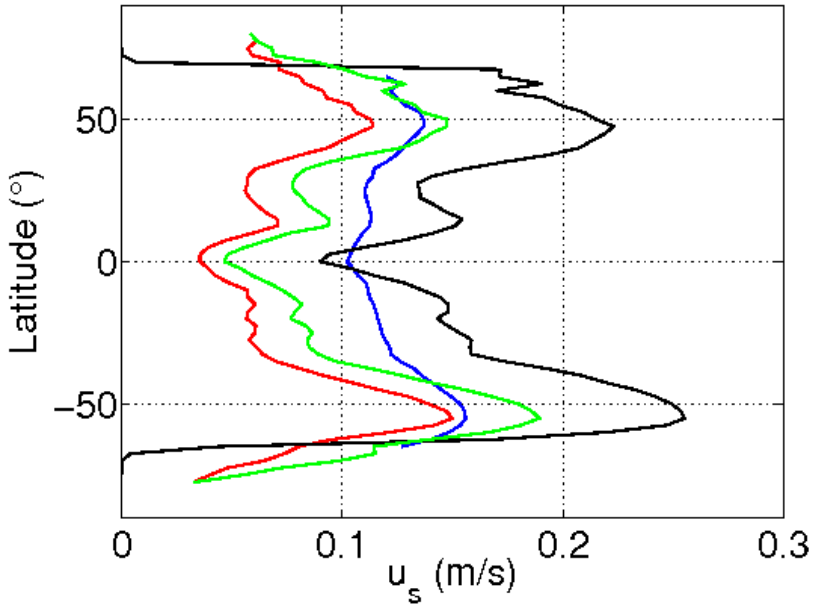

Figure III-10: Surface Stokes drift from TOPEX (blue), ERA40 (red), WW3 (black), and multimodel ensemble climatology (green).

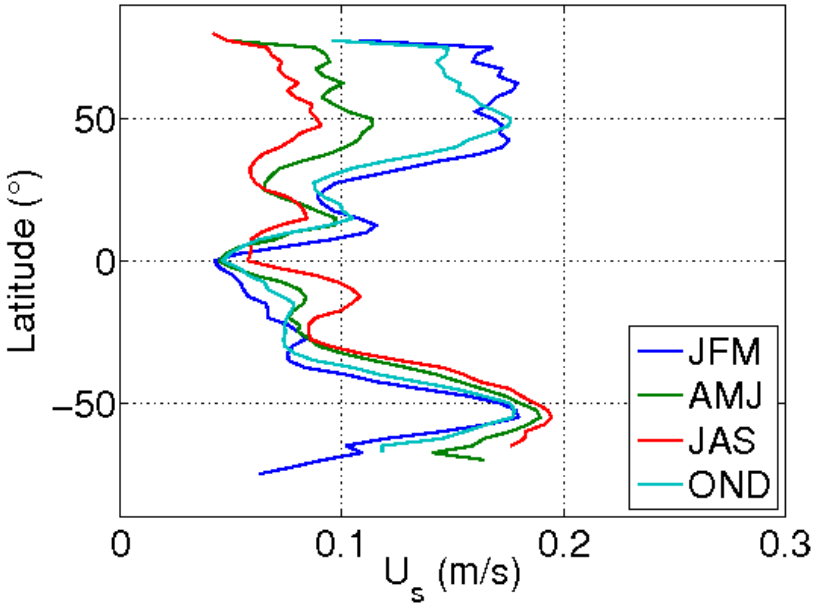

Figure III-11: Seasonal zonal means of Stokes drift from multimodel ensemble

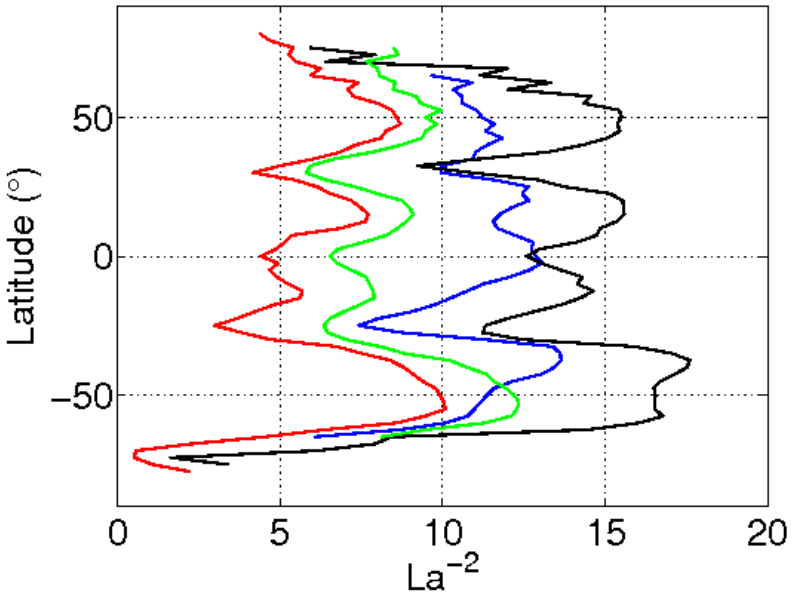

Figure III-12: Inverse-square turbulent Langmuir number from TOPEX (blue), ERA40 (red), WW3 (black), and MME (green)

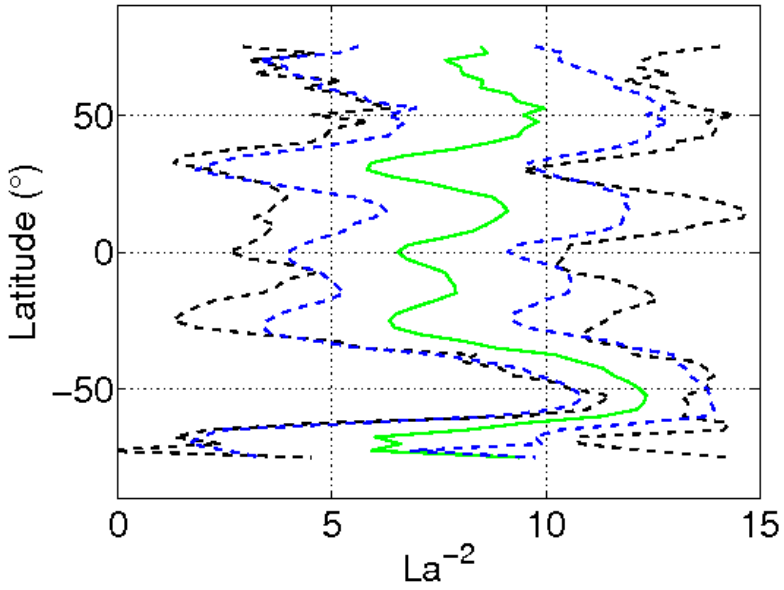

Figure III-13: Multimodel ensemble inverse-square turbulent Langmuir number (solid green) with 2-σ errorbars based on zonal variability (dashed black) and time variability (dashed blue)

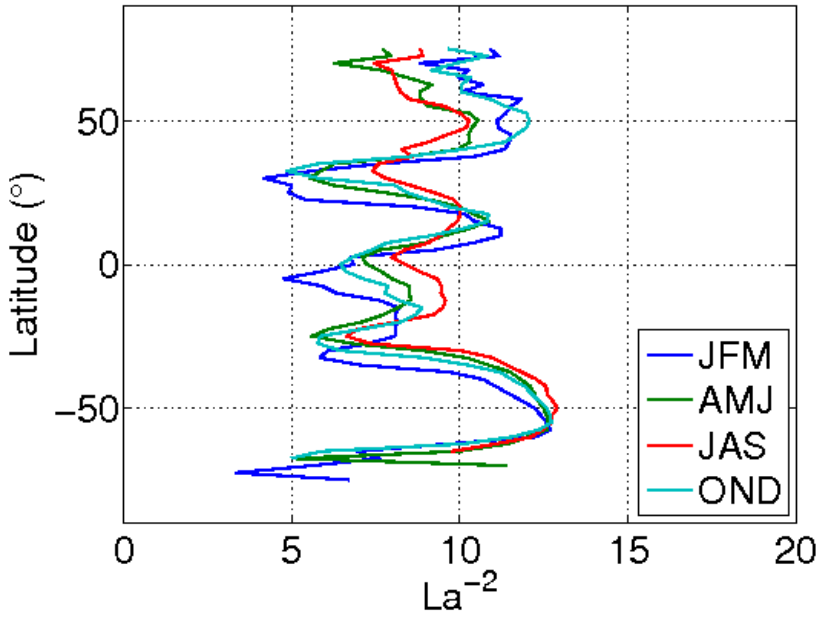

Figure III-14: Seasonal zonal means of inverse square Langmuir Number from multimodel ensemble

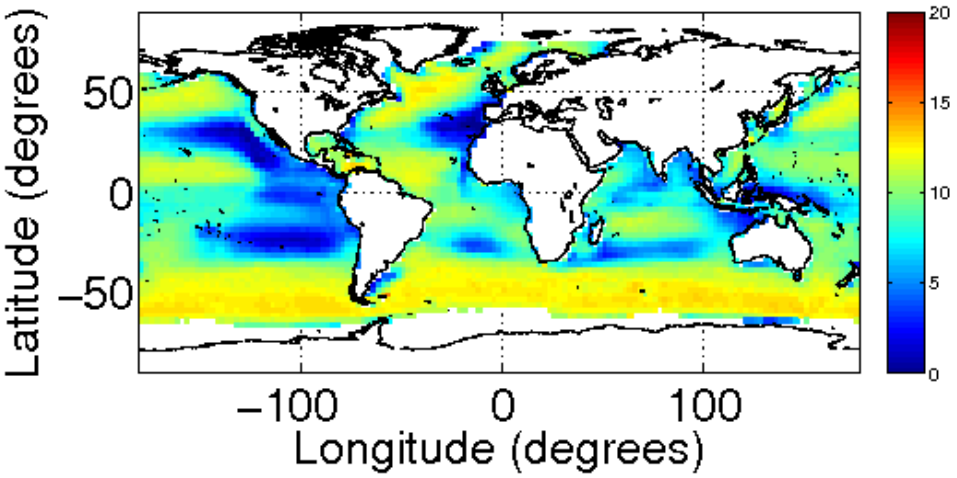

Figure III-15: Global average of multimodel ensemble La^{-2}

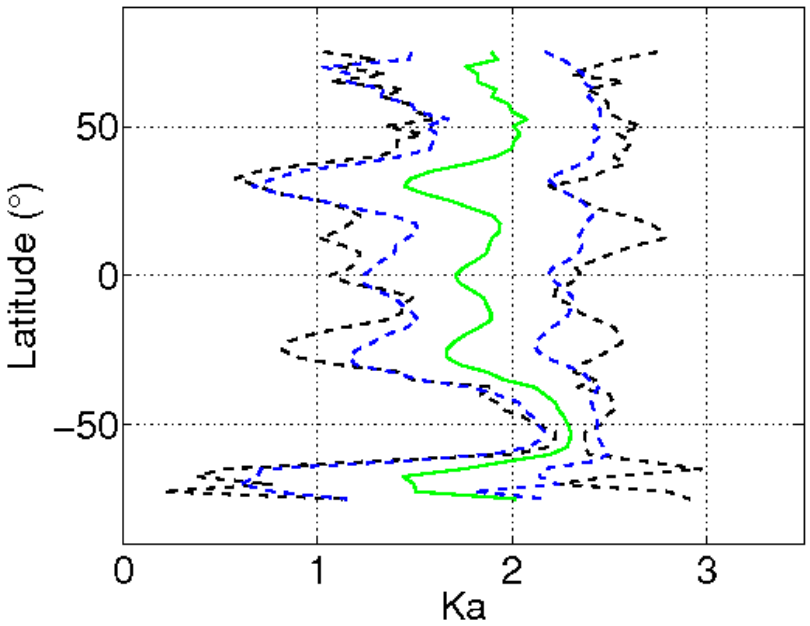

Figure III-16: Multimodel ensemble Kantha number (solid green) with 2-σ errorbars based on zonal variability (dashed black) and time variability (dashed blue)

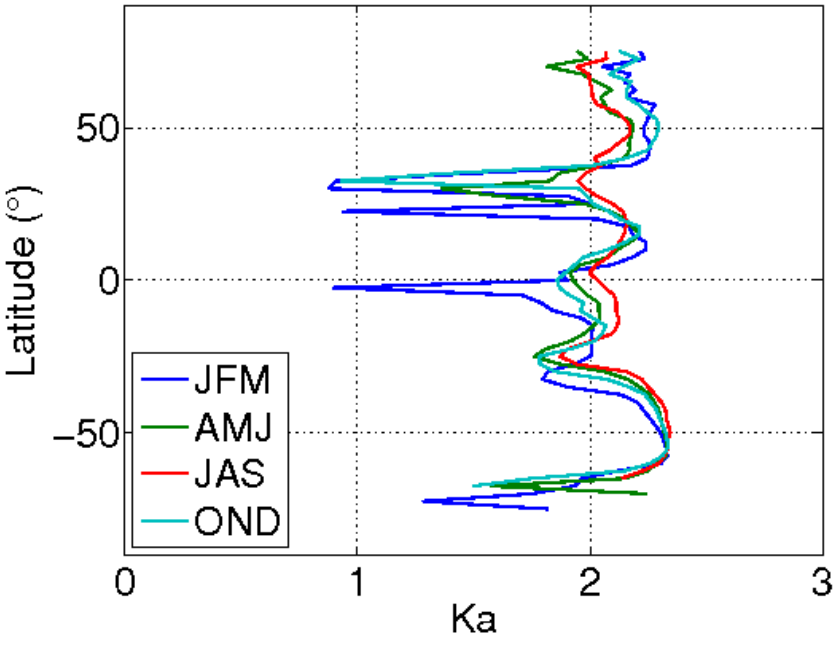

Figure III-17: Seasonal zonal means of Kantha Number from multimodel ensemble

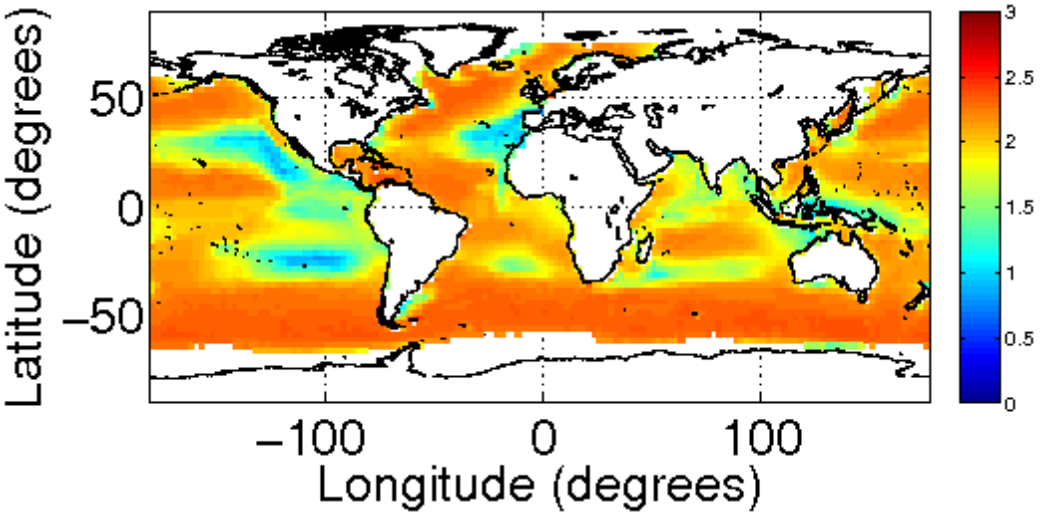

Figure III-18: Map of global average multimodel ensemble Kantha number

IV. DISCUSSION

> "I consider this [the TOPEX/Poseidon mission] the most successful ocean experiment of all times" [1]
>
> - Walter Munk

4.1 Wind Fields and Friction Velocity

To dissect the differences between the ERA40 and WW3 models, we must first look at the wind fields that are forcing these wave models. As discussed in Section II, the wind field from ERA40 comes from the highly-developed ECMWF atmospheric model, while the winds used to force the WW3 model used here are derived from NCEP/NCAR reanalysis (CORE 2.0).

Figure III-2 and Figure III-5 show the small disparity between the two wind fields. The magnitude of the 10-m wind forcing in WW3 is 8.7% higher on average than the ERA40 u_{10} (Figure III-2). Reasons for this slight uncertainty in global average winds are beyond the scope of this study, but the affects are expected to ripple (pun intended) into the modeled ocean wave fields. Wind direction (Figure III-5), however, is nearly identical for both models. This will be important later on when the Langmuir number field is discussed in Section 4.5.

Ocean surface friction velocity, calculated from the ten-meter wind speed by Equation 4, quantifies the momentum transfer between the atmosphere and

[1] From Walter Munk's testimony to the U.S. Commission on Ocean Policy (Walter Munk, 2002, p.2)

ocean. The wind creates waves through this friction velocity, and thus it is the most direct indicator of how the wind is forcing the waves for each data source. As a result of U_{10} being higher in WW3, surface friction velocity is correspondingly higher by 8.8% on average (Figure III-9). While the calculations for friction velocity from wind speed in the two models are different, it is clear that this is not the only reason for the increased u^* in WW3, since the difference is anticipated by the wind speed difference.

4.2 Significant Wave Height

One way to interpret stronger wind forcing in WW3 is that the winds are biased to input more energy into the wave field than ERA40. For example, the wave height and wind speed fields (Figure III-2 and Figure III-3) show a strong correlation, with peaks near 50^o latitude and a lull at the equator. With this in mind, one would expect higher wave heights and shorter wave periods for WW3, and this is exactly what is seen in Figure III-3 and Figure III-4. The significant wave height in WW3 is 24.1% higher, and the mean wave period is 7.5% shorter, than ERA40.

While there is consistency in these numbers and a clear picture of the models is starting to emerge, there is another crucial distinction between ERA40 and WW3. As discussed in Section 2.1.2, ERA40 assimilates ERS altimeter wave height data, thus closely tuning the model output to empirical reality. While this is an advantage in increasing wave height output accuracy, it applies a mysterious cheat, so to speak, bypassing the physical effects to correct the model. This makes

direct comparison between WW3 and ERA40 impossible since our run of WW3 does not assimilate data, and thus has no way to correct for biases due to missing physics. However, the difference between ERA40 and WW3 results is a good indicator of the potential model bias of wave models, and is useful in estimating how much error is expected if WW3 were used as a climate model component to predict future wave climate where data assimilation is unavailable.

Of particular interest are the physics of wave energy transfer to turbulent kinetic energy in the ocean mixed layer. Kantha et al. (2009) has shown that significant energy is extracted from the wave field by Stokes production of turbulent kinetic energy. This energy exchange is a consequence of Stokes drift, which is described in more detail in Section 1.2. If Stokes production in fact accounts for a large amount of energy removed from the wave field (as predicted by Kantha et al., 2009), then this mechanism might explain some of the extra energy in the WW3 wave field. I strongly encourage future studies to determine the contribution of Stokes production to the discrepancy between models with and without data assimilation.

The effects of data assimilation into a model are clearly evident in Figure II-1, as discussed in Section 2.1.2. It is not surprising to see ERA40 wave heights agree quite well (average difference 4.9%) with TOPEX altimetry, since TOPEX is essentially a different version of the same altimeter technology used in ERS 1 and 2, the data from which are assimilated into ERA40. The strong agreement lends weight to the superiority of these wave height fields over that of the non-

assimilating WW3, despite its advancements compared to other models (as reported in Section 2.1.3).

4.3 Mean Wave Period

Figure III-4 shows the second-moment mean wave period climatology calculated from each source. The spread between the sources tells of the level of uncertainty in the global wave period field. However, Caires et al. (2005) reports strong biases in TOPEX T_m derived from the Gommenginger et al., (2003) model in swell-dominated seas with low winds. One would then expect the regions of highest disagreement in T_m to correlate well with regions that are climatologically swell-dominated with weak winds. In fact, a side-by-side comparison of wave age and wind speed with ERA40-TOPEX T_m difference reveals that all areas of large T_m disagreement occur within swell-dominated regions with low winds, as expected (Figure IV-1).

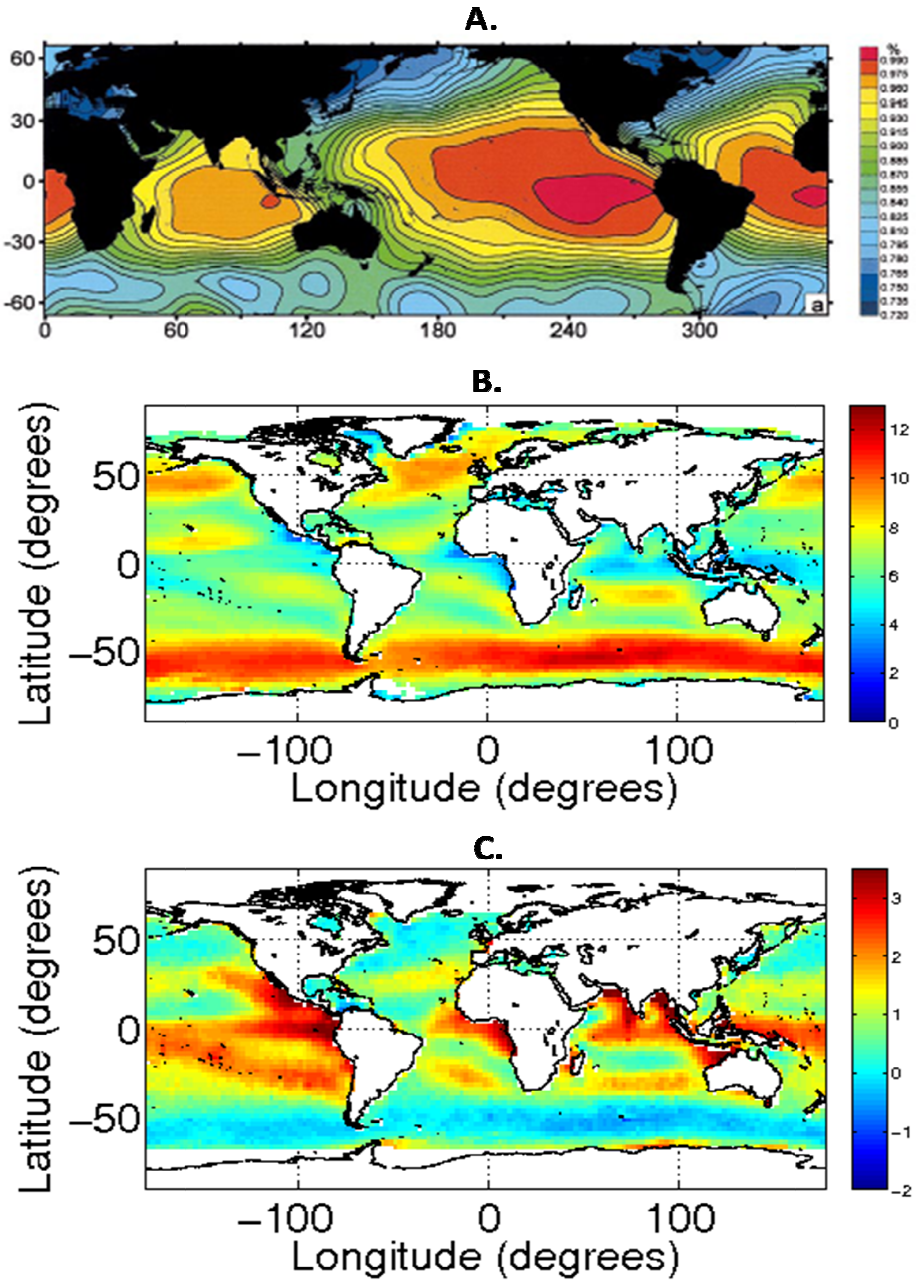

Figure IV-1: **A)** Global swell-sea probability from Chen et al. (2002), (the color scale goes from 72 - 99%). **B)** Average 10-meter wind speed from ERA40 [m/s]. **C)** ERA40-TOPEX average difference in mean wave period [s].

There are regions in Figure IV-1 in which TOPEX and ERA40 agree quite well in wave period, even though swell seas dominate climatologically. The most

conspicuous of these regions is in the central Pacific between the equator and the Hawaiian Islands. Though this region has large swell (Figure IV-1 A), wave period (Figure IV-1 C) is accurately resolved in the TOPEX data because of the higher wind speeds common to the area (Figure IV-1 B). This confirms the assertions (that both swell climate and wind speed must be considered to quality control TOPEX data) made by Caires et al. (2005). There are no significant regions of wave period disagreement in climatologically wind-dominated regions. The wave period disagreement, like the swell climatology, hugs the eastern ocean boundaries, staying within roughly 30^{o} of the equator.

4.4 Stokes Drift

The average surface Stokes drift from each data source is shown in Figure III-10. The disagreement between sources is problematic because it translates into increased uncertainty in the magnitudes of factors resulting from Stokes Drift, such as production of turbulent kinetic energy. Stokes drift (Eqs. 6 and 7) is highly sensitive to wave height errors and extremely sensitive to errors in mean wave period due to the respective powers of 2 and 3 in the Stokes drift equation. The result is that small errors or disagreement in wave height and wave period are magnified in Stokes drift. Comparison of Figure II-2 and Figure III-10 shows that wave period disagreement is the primary source of uncertainty in Stokes drift, where WW3 is 40.2% and 88.3% higher worldwide than TOPEX and ERA40 respectively. It is counterintuitive that WW3 is closer to TOPEX than ERA40 in its calculation of U_s, since the TOPEX data has a clear and known low bias for

wave period (See Section 2.1.1). However, WW3 has an apparent high significant wave height bias as discussed above.

The final Stokes drift climatology (Figure III-10, Figure III-11, and Appendix A) was calculated from the multimodel ensemble wave height and wave period fields. The seasonal average U_s (Figure III-11) shows a clear seasonal signal: the stokes drift is more than twice as strong in the Northern hemisphere in the winter months than in the summer months. This trend is expected since wind and storm activity increases in this area during winter, but the magnitude of the seasonal signal is dramatic. Interestingly, the seasonal U_s signal remains in the La^{-2}/Ka climatologies (Figure III-14 and Figure III-17), though its relative magnitude is less pronounced, as wintertime u^*increases along with Stokes drift. This suggests that the U_s and u^* seasonal signals are different enough to change the Langmuir mixing climate seasonally.

4.5 Langmuir and Kantha Numbers

The level of disagreement seen in U_s (40.2% and 88.3% for WW3-TOPEX and WW3-ERA40 respectively) translates directly into equal uncertainty in La^{-2} (40.2% and 88.3% respectively), but to only cube-root uncertainty in Ka (11.9% and 23.5% respectively). This example shows one advantage of using the Kantha number to describe Langmuir mixing conditions: the uncertainty between the models and observations, which is doubled or tripled in the calculation of U_s, is then divided nearly back to the original percentage of uncertainty. This increase

in confidence of the resulting Kantha number climatology nicely compliments the physical logic behind the Kantha number as compared to the Langmuir number.

However, histograms of La, La^{-2}, and Ka (Figure IV-2) reveal La^{-2} to have the most normal distribution. The resulting advantage is that using standard deviation to estimate statistical variability for $La^{-2}$is more appropriate than for Kantha number. This less-skewed distribution is an important factor to consider when choosing among these parameters to measure wind-wave equillibrium. Even more important is the realization that the averages of the three Langmuir-related definitions used here (Eqs. 1) will each be warped according to the unique skewness and kurtosis (tail weight and stoutness) of the differing distributions. Also, the 2σ error bounds included in Figure III-13 and Figure III-16 are only representative scatter in Gaussian-distributed data, and thus can be trusted more in the case of La^{-2}. That said, sometimes a Gaussian distribution is not the most realistic distribution, and in cases such as this normal standard deviations are not a good way to represent variability. Whether the Langmuir number distribution should, in theory, be Gaussian is an open question at this point.

To demonstrate the effect of the distribution shapes, Table IV-1 shows the mean, median, skewness, and kurtosis (where 3.0 = Gaussian) of each distribution.

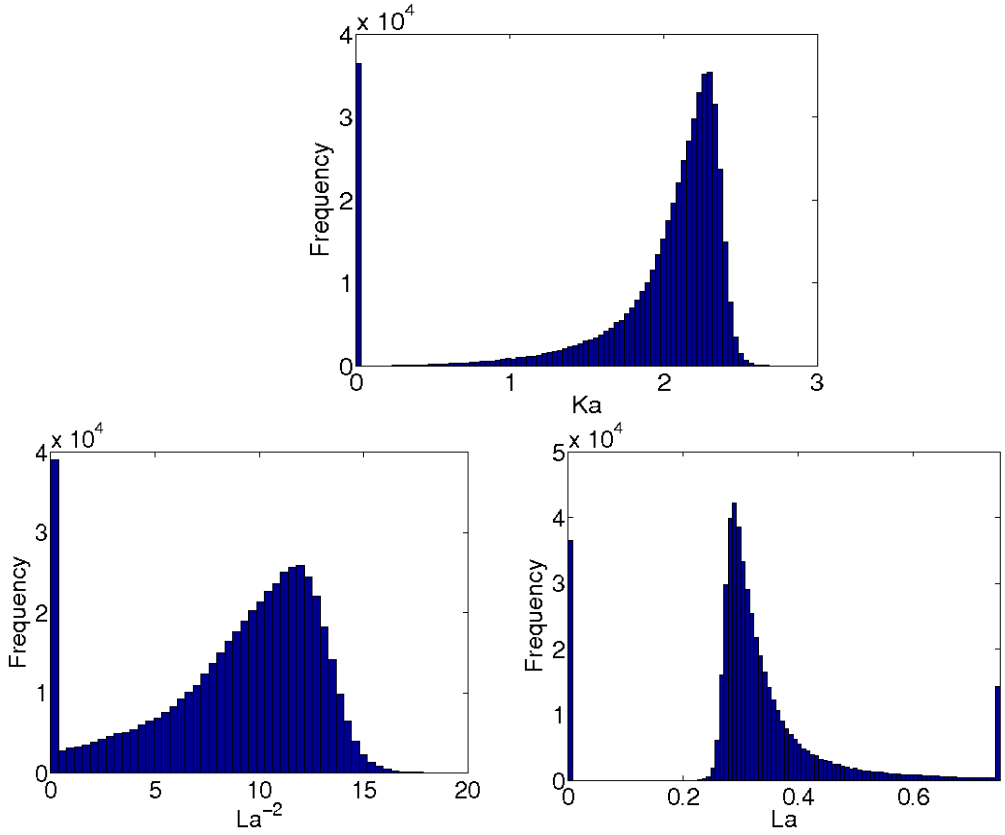

Figure IV-2: Histograms of La, Ka, and La-2

Table IV-1: Langmuir/Kantha number statistics

Variable	Mean	Median	Skewness	Kurtosis
La	0.33	0.31	0.36	6.02
La^{-2}	8.78	9.78	-0.79	2.77
Ka	1.92	2.14	-2.19	7.02

Figure III-15 and Figure III-18 show the final climatologies of La^{-2} and *Ka*. The regions of low activity in these figures are caused by local climatological

misalignment of the wind and waves, as seen in Figure III-8. It is notable that the same regions of wind/wave misalignment are characterized by low (<5 m/s) average winds (Figure IV-1 B). The emerging picture is that low winds combined with strong remotely generated swell provide misalignment between the wind and waves, and thus the mechanism by which Langmuir number is decreased. In nearly all other regions of the global ocean, the strength of the surface wind stress, Stokes drift, and the alignment between the two are conducive to Langmuir cell formation and/or strengthening ($La^{-2} \sim 11$ or $Ka \sim 2.25$). Areas of overall light winds or equatorward trade winds are the only areas of diminished Langmuir mixing likelihood across the world's oceans.

The climatology (Figure III-18) shows that 77.2% of the Earth's ocean surface has a Kantha number greater than 1.75 ($La < 0.43$, $La^{-2} > 5.4$). Regions of especially high Kantha number include the stormy regions of the world, aligned in near zonal belts at roughly 50°S, 20°N, and 50°N.

Langmuir number variability in time and space (Figure III-13) is comparable, though slightly less temporally than it is zonally. Variability is much less in the southern ocean than across the rest of the world, and this is due to a lack of continental boundaries and persistent storminess there year round. Comparison of Figure III-12 and Figure III-13 shows that the final Langmuir number disagreement between the three data sources is generally within the temporal and regional scatter.

The highest Kantha numbers are in the Southern ocean. There, strong and consistent westerly flow with imbedded polar front cyclones generates strong surface winds, driving large swell. This very active region of the ocean is also the location of the persistent mixed layer depth shallow bias in climate models. It is possible that correctly including Langmuir mixing into the models will help to decrease this known bias. Research into the effect of Langmuir mixing on model mixed layer depth is ongoing and tangential to this study, but preliminary work by Webb et al. (2010) shows the potential usefulness of a Langmuir mixing climatology such as this one.

V. CONCLUSIONS AND RECOMMENDATIONS

5.1 Conclusions

This study has looked through large amounts of oceanographic data from three different sources in order to determine the spread that exists between the sources. Section III displayed a summary of the data, and a more complete view is found in Appendix A.

Three different definitions of Langmuir number have been studied here, each with its own merits. Indeed the researcher may choose the definition that best suits his purposes, with one exception. Any definition of *La* for which the ratio of Stokes drift to friction velocity is raised to a power, special care must be taken to account for the resulting skewing of the data distribution. Conclusions drawn from simple statistics computed from these skewed distributions may be inaccurate.

The multilmodel ensemble climatology presented here considers each source's strengths and weaknesses to create a blended best guess at the true wave field. The MME climatology shows significant Langmuir mixing conditions to exist over most of Earth's oceans, with the only regions of inactivity being in tropical trade wind areas. The strength of the average Kantha number worldwide is estimated at ~2.25 (La~0.3, La^{-2}~11.4) in the vast regions of aligned wind and waves and strongest in the stormy Southern ocean. This value of Langmuir number suggests that Langmuir mixing is likely to be strong and common worldwide. The potential effects this may have on climate projection is an open

question, since model sensitivity to Langmuir mixing inclusion has already been shown. More important than the inclusion of Langmuir mixing in models is the accuracy of the strength and depth of the mixing. While this study suggests Langmuir mixing to be significant, the scatter of possible correct values of the average Langmuir number field ($6 < La^{-2} < 13$ zonally), as well as its temporal and spatial spread, will likely have a drastic affect on Langmuir mixing depth in models. For this reason, any model including Langmuir mixing based on climatology should be tested at the extremes of the *La* scatter to determine the level of confidence in the output solution.

One group of variables is well-agreed upon by all three sources (average disagreement 10% or less). This group includes significant wave height, ten-meter wind speed and direction, surface friction velocity, and wave direction. Wave height and wind speed have been accurately mapped by satellites and validated with in situ observations, and this foundation of high accuracy is included into the models through assimilation. This study confirms the importance of data assimilation in models, showing how it can be used to bypass missing physics or crude parameterizations.

However, variables that cannot be assimilated into the models because they are not well-measured empirically (mean wave period, Stokes drift, and Langmuir/Kantha number) represent a group of data for which there is large disagreement between sources. The level of scatter for wave period shows its calculation and worldwide measurement accuracy is behind that of other wave

parameters. While buoy data can help to ensure the models agree in localized regions, they cannot help describe the worldwide climate at their current infrastructure. The only way to reconcile the scatter between the sources looked at here is to gather more observations. Until then, neither can be given any more weight than another when considering the total world ocean climate, even though some may outperform others in certain regions of the world or in certain conditions. There is hope that improved altimeter-derived wave period measurement can alleviate this problem in the near future, but at present the altimeter wave period is even less trustworthy than the models.

The ERA40 and WW3 wave height and period data suggest there is a missing piece in present wave model physics. The WW3 field has higher energy on average, and this may be due a combination of factors including missing dissipation of wave energy from Stokes production of turbulent kinetic energy. Since the WW3 run used here does not assimilate data, it has no way to tune past any possible missing physics like ERA40 can. This distinction reveals something about the level of correctness of the model physics, as well as the operational use of the WW3 model. If WW3 is to be run in the future, I highly recommend assimilating wave field data when possible. Even the most sophisticated model seems to be no match for empirical observations where they exist. Indeed it is the model's job to fill in the gaps in the empirical data record, but the extent to which we trust the model data should be based on the density of the points assimilated and not necessarily the strength of the model physics.

The multimodel ensemble presented here is nice way to collapse the data scatter into one climatology, however I caution the user of this data not to fully trust it as more accurate than the data from one source alone. There is no way to know whether the MME average is more or less correct than each source. Instead, the MME serves to show not just a best guess at what is correct, but the bigger picture including the total amount of knowledge spread in the parameter space. By increasing the amount and variety of data used to create a climatology, we only improve our total understanding of the range of possible correct answers. Much information would be missed by only considering data from ERA40, for example. But by looking at two additional sources the ERA40 data can be put into the context of the state of present ocean characteristic knowledge. Essentially, by only using one data source, we are unaware of what we don't know.

5.2 Recommendations for Future Work

The next logical step forward is to include the new Langmuir climatology and its spread into a climate model. Work to achieve this is currently being carried out by Baylor Fox-Kemper, Adrean Webb, and the author at the University of Colorado, Boulder. It may be that the current amount of spread in the Langmuir field leads to differing climate solutions that are unsatisfactory. If this is the case, refinement to this climatology must be made. There are a few other data sources that could be brought in to further increase the accuracy of the multimodel ensemble mean.

ARGO floats measure temperature and salinity profiles over a wide range of the ocean in its upper layers. The mixed layer depth can be computed from these profiles, and it may be possible to incorporate such data with data from the climatology presented here to more accurately determine the true mixed layer depth on large scales. Additionally, buoy data can be used to further validate wave period and height after accounting for positioning biases.

An investigation into the differences between various levels of data-assimilating and non-assimilating models may shed light on the missing or incorrect physics. Until the models can accurately map the oceans without any data assimilation past its initial conditions, much could be learned about what is missing by assimilating data in chunks. One example shown in this study is Stokes production of turbulent kinetic energy, and the underestimate in wave dissipation in the non-assimilating WW3 model, which could be due to omission of this effect (although it is also likely that the ad-hoc parameterization of wave dissipation in the model could be adjusted to account for the underestimation).

Finally, worldwide average wave period seems to be the main piece of basic wave data that is still rather uncertain. Further campaigns to measure this quantity on a global, climate scale could greatly improve ocean wave modeling and research. Perhaps in the future a robust instrument or technique will allow direct wave period measurement on this scale from a remote sensing satellite. Such data would have greatly reduced the scatter of the Langmuir number and Stokes drift estimates in this study, were they available.

VI. REFERENCES

Banner, M.L., A.V. Babanin, and I.R. Young, 2000: Breaking Probability for Dominant Waves on the Sea Surface. *J. Phys. Oceanogr.*, 30, 3145–3160.

Bidlot, J-R, D.J. Holmes, P.A. Wittman, R. Lalbeharry, and H.S. Chen, 2002: Intercomparison of the Performance of Operational Ocean Wave Forecasting Systems with Buoy Data. *AMS J. Weather and Forecasting*, 17, 287-310.

Caires, S., A. Sterl, J.R. Bidlot, N. Graham, and V. Swail, 2004: Intercomparison of Different Wind–Wave Reanalyses. *J. Climate*, 17, 1893–1913.

Caires S., A. Sterl, and C.P. Gommenginger, 2005: Global Ocean Mean Wave Period Data: Validation and Description. *J. Geophys. Res.*, 110, CO2003, doi:10.1029/2004JC002631.

Cavaleri, L., J. H. G. M. Alves, F. Ardhuin, A. Babanin, M. Banner, K. Belibassakis, M. Benoit, M. Donelan, J. Groeneweg, T. H. C. Herbers, P. Hwang, P. A. E. M. Janssen, T. Janssen, I. V. Lavrenov, R. Magne, J. Monbaliu, M. Onorato, V. Polnikov, D. Resio, W. E. Rogers, A. Sheremet, J. M. Smith, H. L. Tolman, G. van Vledder, J. Wolf, and I. Young: 2007, Wave modelling - the state of the art. *Progress In Oceanography*.

Chelton D. B., E. J. Walsh, and J. L. MacArthur, 1989: Pulse compression and sea level tracking in satellite altimetry. *J. Atmos. Oceanic Technol.*, **6**, 407–438.

Chen, G., B. Chapron, R. Ezraty, and D. Vandemark, 2002: A Global View of Swell and Wind Sea Climate in the Ocean by Satellite Altimeter and Scatterometer. *J. Atmos. Oceanic Technol.*, **19**, 1849–1859.

D'Asaro, E.A. and G.T.Dairiki, 1997: Turbulence Intensity Measurements in a Wind-Driven Mixed Layer. *J. Phys. Oceanography*, 27: 2009-2022.

Gommenginger, C.P., M.A. Srokosz, P.G. Challenor, and P.D. Cotton, 2003: Measuring ocean wave period with satellite altimeters: A simple empirical model. *Geophys. Res. Letters*, 30(22), 2150.

Gourrion, J., D. Vandemark, S. Bailey, B. Chapron, C.P. Gommenginger, P.G. Challenor, and M.A. Srokosz, 2002: A two parameter wind speed altimeter for Ku-band altimeters, *J. Atmos.OceanicTechnol.*, 19(12), 2030-2048.

Harcourt, R. R. and E.A. D'Asaro, 2006: Large Eddy Simulation of Langmuir Turbulence in Pure Wind Seas. *AGU Fall Meeting Abstracts*, A562+.

Hanson, J. L., B. A. Tracy, H. L. Tolman and R. D. Scott, 2009: Pacific hindcast performance of three numerical wave models, *J. Atmos. Oceanic Techn.*, In Press.

Hwang, P.A., W.J. Teague, G.A. Jacobs, and D.W. Wang, 1998: A Statistical Comparison of Wind Speed, Wave Height, and Wave Period from Satellite Derived Altimeters and Ocean Buoys in the Gulf of Mexico Region. *J. Geophysical Res.*, 103, 10451-10468.

Johnson, H.K., J. Højstrup, H.J. Vested, and S.E. Larsen, 1998: On the Dependence of Sea Surface Roughness on Wind Waves. *J. Phys. Oceanogr.*, 28, 1702–1716.

Kantha, L. and C. Clayson: 2004, On the effect of surface gravity waves on mixing in the oceanic mixed layer. *Ocean Modelling*, 6,101-124.

Kantha, L. and C. Clayson, Small Scale Processes in Geophysical Fluid Flows. London: Academic Press, 2000.

Kantha, L., P. Wittmann, M. Sclavo, and S. Camiel, 2009: A preliminary estimate of the Stokes dissipation of wave energy in the global ocean. *Geophys. Res. Letters*, VOL. 36, L02605, doi:10.1029/2008GL036193.

Kantha, L. H., U. Lass, and H.Prandke, 2010: Stokes production of turbulence kinetic energy in the oceanic mixed layer: Observations in the Baltic Sea, Ocean Dynamics, 60, 171-180. **DOI: 10.1007/s10236-009-0257-7.** (seeDOI 10.1007/s10236-010-0283-5 for errata, which includes correct definition of Kantha number Ka).

Komen, G.J., L. Cavaleri, M. Donelan, K. Hasselmann, S. Hasselmann, P. Janssen, 1994: Dynamics and Modelling of Ocean Waves. Cambridge University Press: Cambridge.

Large, W. R., and S.G. Yeager, 2008: The global climatology of an interannually varying air-sea flux data set. *Climate Dynamics*. (Submitted).

Li, M. and C. Garrett, 1997: Mixed layer deepening due to Langmuir circulation. *Journal of Physical Oceanography*, 27, 121-132.

Li, M., K. Zahariev, and C. Garrett, 1995: Role of Langmuir circulation in the deepening of the ocean surface mixed-layer. *Science*, 270, 1955-1957.

McWilliams, J. C. and P. P. Sullivan, 2001: Vertical mixing by Langmuir circulations. *Spill Science & Technology Bulletin*, 6, 225-237.

McWilliams, J. C., P. P. Sullivan, and C.-H. Moeng, 1997: Langmuir turbulence in the ocean. *Journal of Fluid Mechanics*, 334, 1-30.

McWillimas, J.C. and J.M. Restrepo, 1999: The Wave-Driven Ocean Circulation. *J. Phys. Oceanography*, 29, 2523-2540.

Munk.W.: Testimony Before the U.S. Commission on Ocean Policy, April 2002, <http://www.oceancommission.gov/meetings/apr18_19_02/munk_statement.pdf>.

NCEP EMC Martine Modeling and Analysis Branch. WAVEWATCH III MODEL http://polar.ncep.noaa.gov/waves/wavewatch/wavewatch.shtml (Accessed March 20th, 2010).

Plueddemann, A.J., J. A. Smith, D. M. Farmer, R. A. Weller, W. R. Crawford, R. Pinkel, S. Vagle, and A. Gnanadesikan, 1996: Structure and variability of Langmuir circulation during the surface waves processes program. *Journal of Geophysical Research-Oceans*, 101, 3525-3543.

Rosenzweig, C., G. Casassa, D.J. Karoly, A. Imeson, C. Liu, A. Menzel, S. Rawlins, T.L. Root, B. Seguin, P. Tryjanowski, 2007: Assessment of observed changes and responses in natural and managed systems. *Climate Change 2007: Impacts, Adaptation and Vulnerability.Contribution of Working Group II to the Fourth Assessment Report of the Intergovernmental Panel on Climate Change*, M.L. Parry, O.F. Canziani, J.P. Palutikof, P.J. van der Linden and C.E. Hanson, Eds., Cambridge University Press, Cambridge, UK, 79-131.

Smith, J. A., 1998: Evolution of Langmuir circulation during a storm. *Journal of Geophysical Research-Oceans*, 103, 12649-12668.

Smyth, W.D., E.D. Skyllingstad, G.B. Crawford, and H. Wijesekera, 2002: Nonlocal Fluxes and Stokes drift effects in the K-profile parameterization. Ocean Dynamics, 52: 104–115.

Sterl, A. and S. Caires, 2005: Climatology, variability and extrema of ocean waves: the Web-based KNMI/ERA-40 wave atlas. *Int. J. Climatol.* 25: 963–977.

Sullivan, P.P. and J.C. McWilliams, 2010: Dynamics of Winds and Currents Coupled to Surface Waves. *Annual Review of Fluid Mechanics*. 42, 19-42.

Tolman, H.L., 2002: Validation of WAVEWATCH III version 1.15 for a global domain. NOAA / NWS / NCEP / OMB Technical Note Nr. **213**, 33 pp.

Vandemark, D., J.B. Edson, B. Chapron, 1996: Altimeter estimate of sea surface wind stress for light to moderate winds. *J. Atmos. Oceanic Technol.*, 14(3), 716-722.

Wang, X.L., and V.R. Swail, 2001: Changes of Extreme Wave Heights in Northern Hemisphere Oceans and Related Atmospheric Circulation Regimes. *J. Climate*, 14, 2204–2221.

Webb, A., B. Fox-Kemper, W.G. Large, and S. Peacock (2010): Demonstrated sensitivity to Langmuir mixing in a global climate model, *Eos Trans. AGU*, 91(26), Ocean Sci. Meet. Suppl., Abstract PO31B-04.

Weller, R. A. and J. Price, 1988: Langmuir circulation within the oceanic mixed layer. *Deep-Sea Research*, 35, 711-747.

VII. APPENDIX A: SEASONAL CLIMATOLOGY

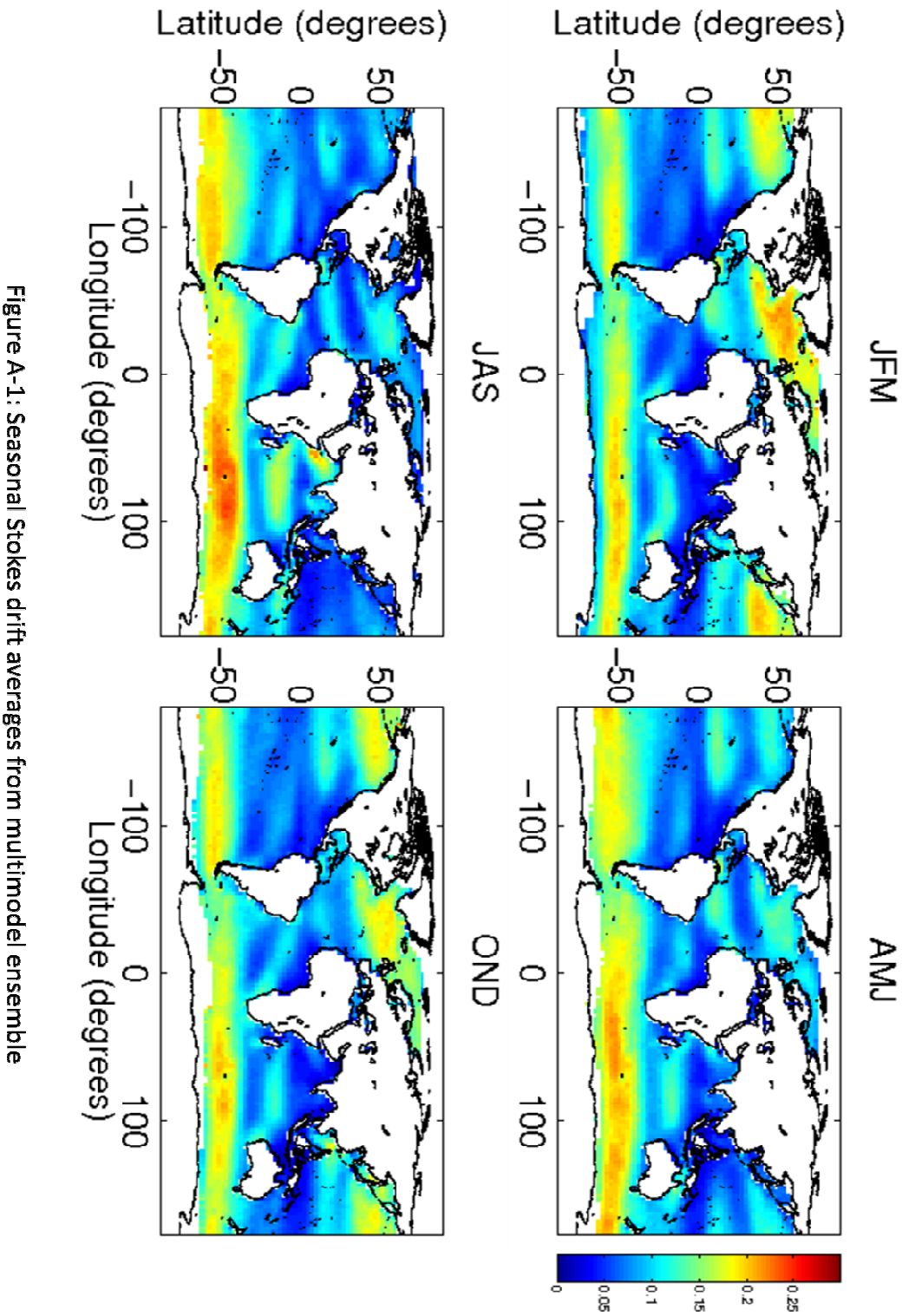

Figure A-1: Seasonal Stokes drift averages from multimodel ensemble

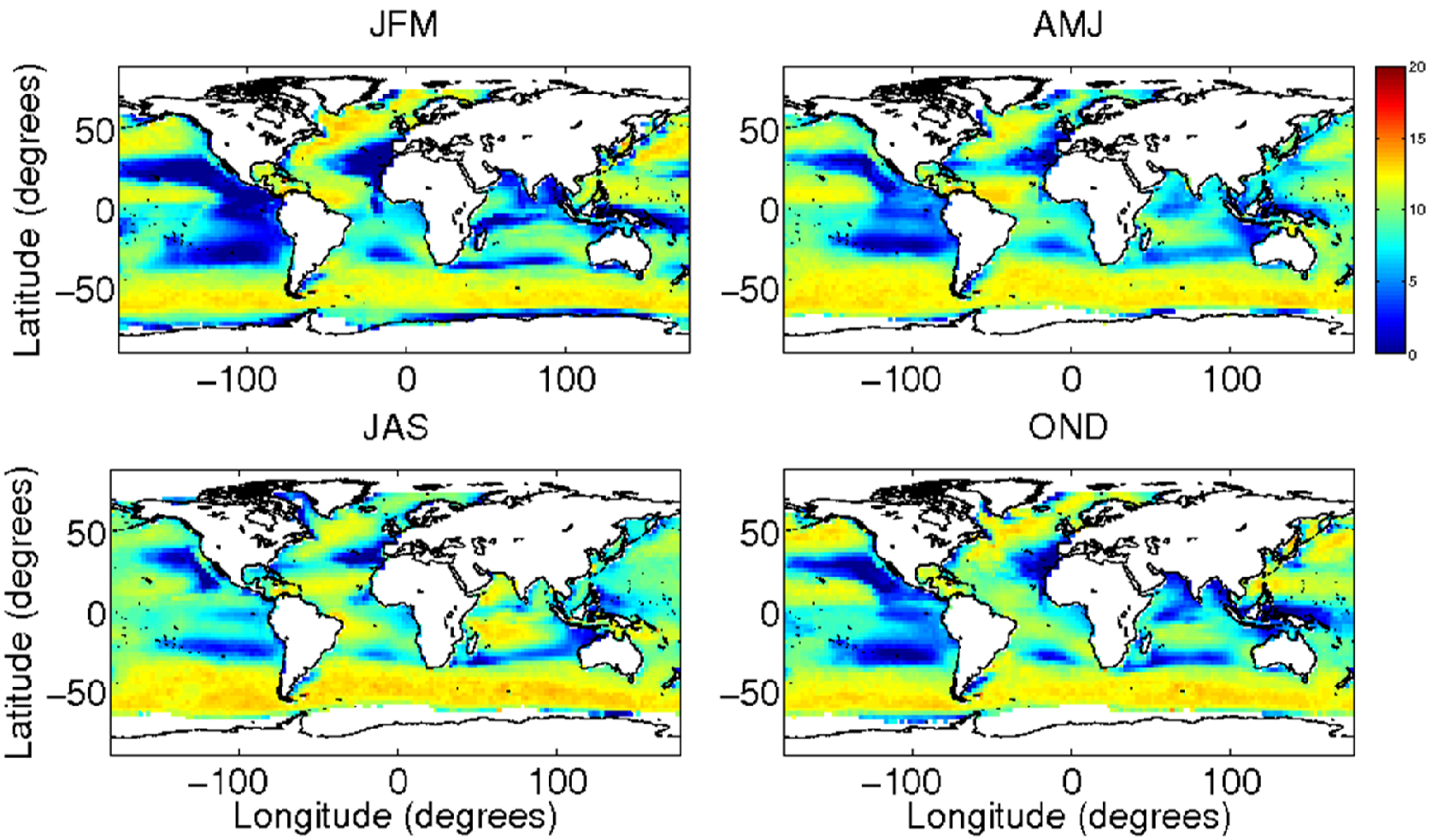

Figure A-2: Seasonal Langmuir number averages from multimodel ensemble

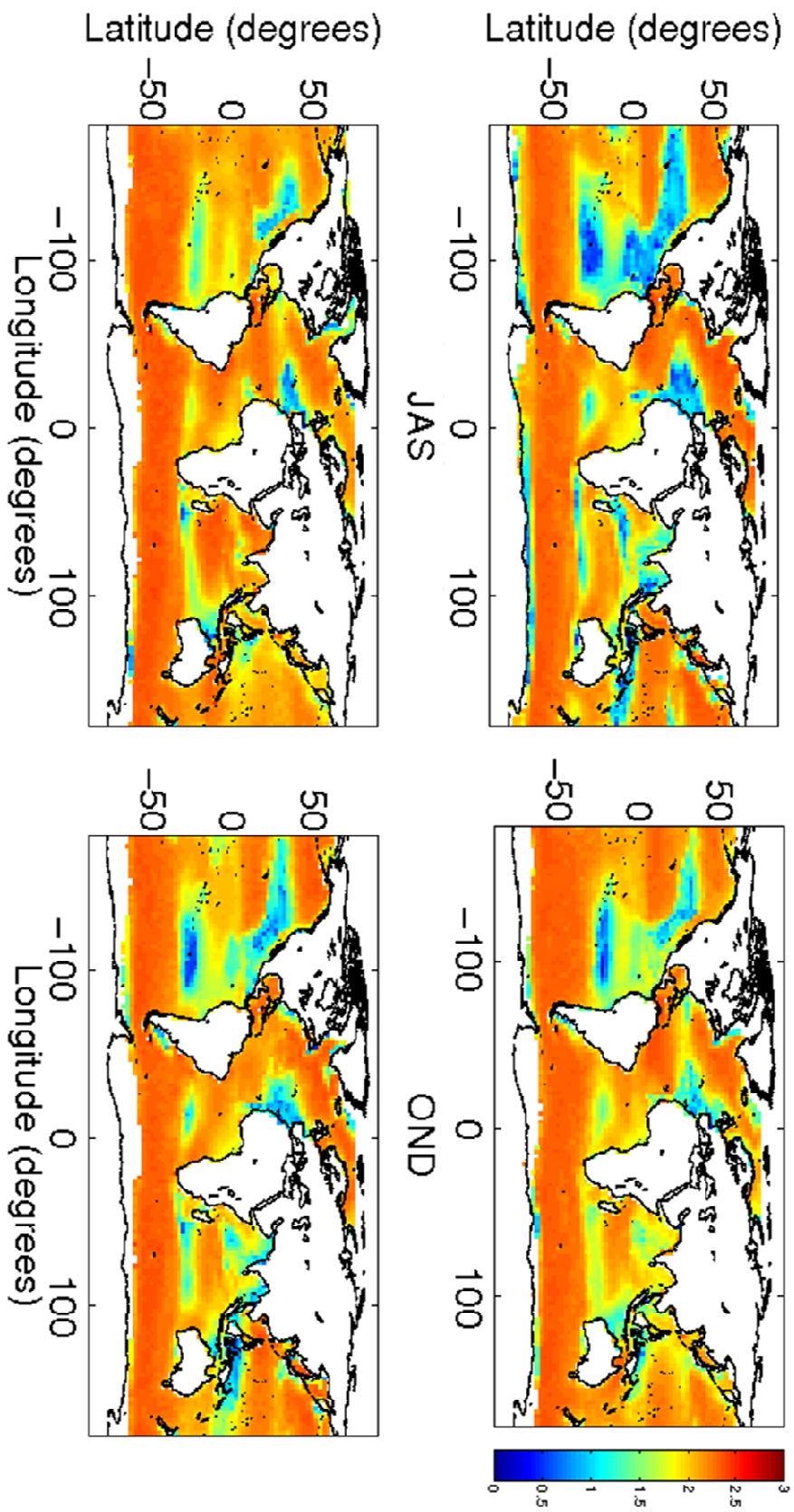

Figure A-3: Seasonal Kantha number averages from multimodel ensemble

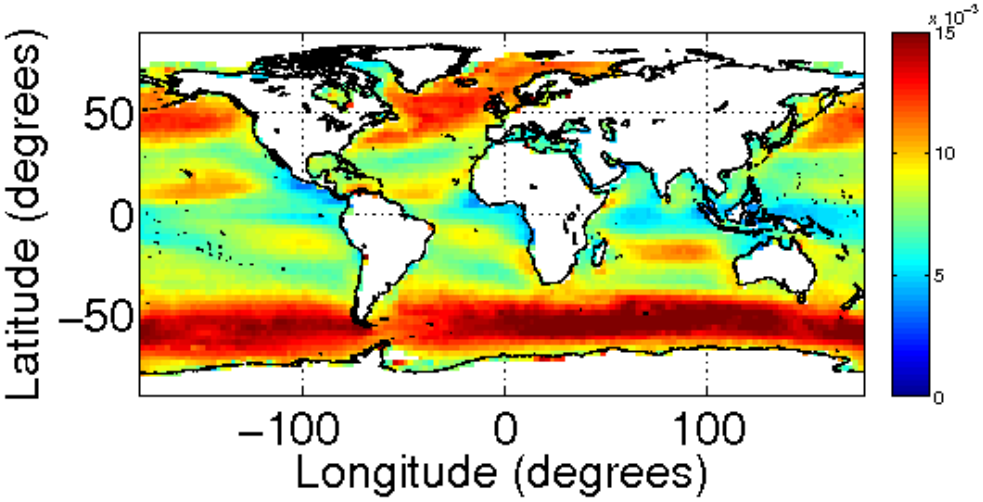

Figure A-4: Average friction velocity from multimodel ensemble

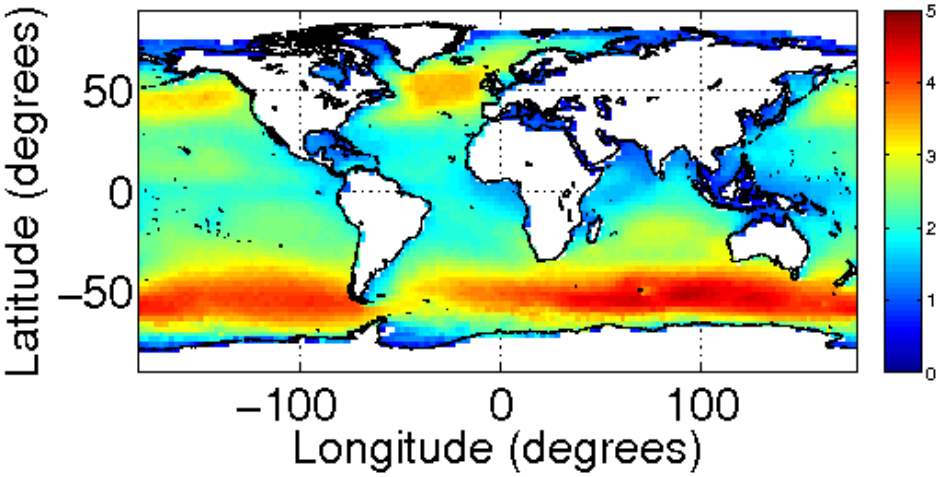

Figure A-5: Average significant wave height from multimodel ensemble

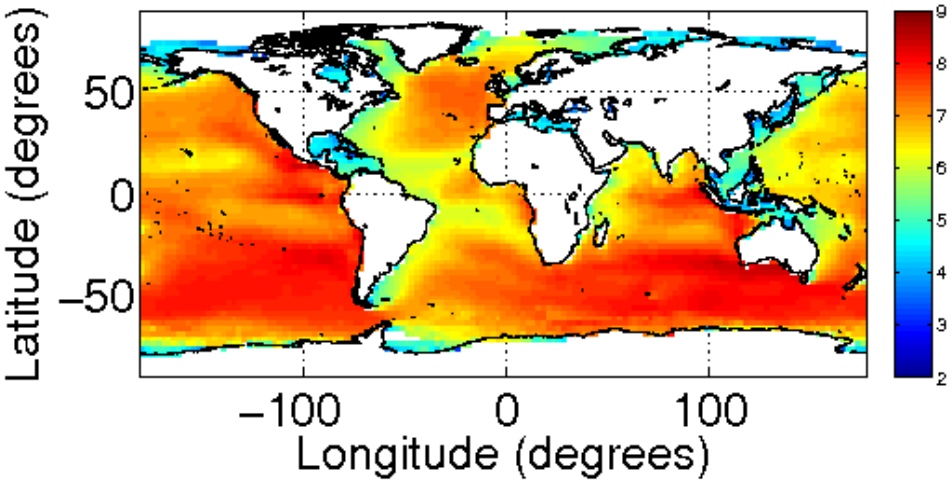

Figure A-6: Average mean wave period from multimodel ensemble

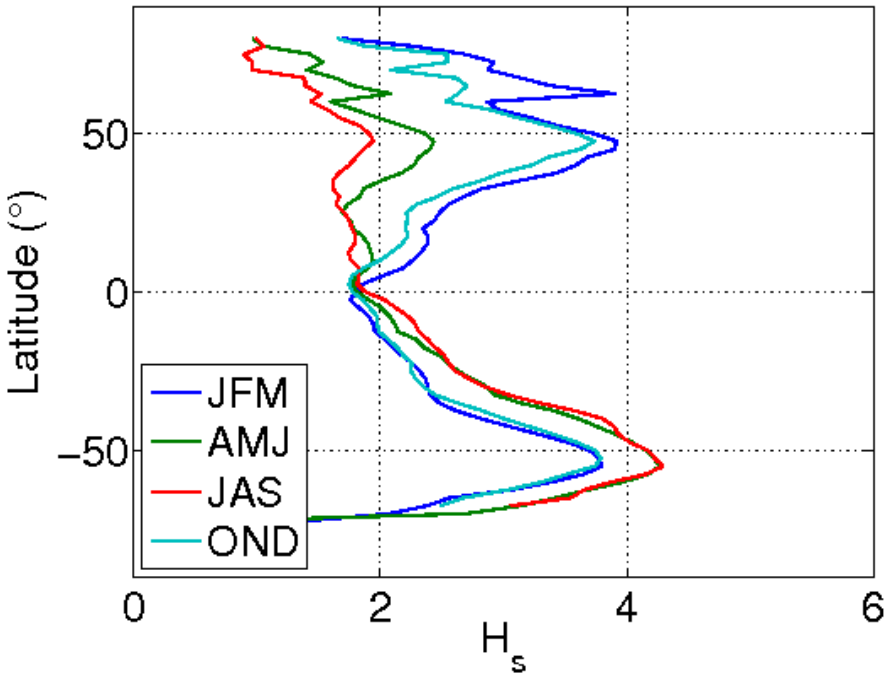

Figure A-7: Seasonal zonal average significant wave height from multimodel ensemble

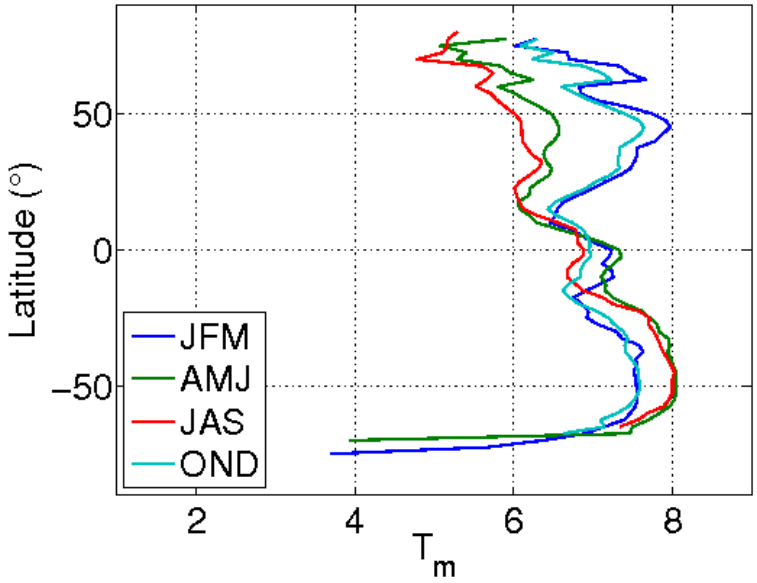

Figure A-8: Seasonal zonal average mean wave period from multimodel ensemble

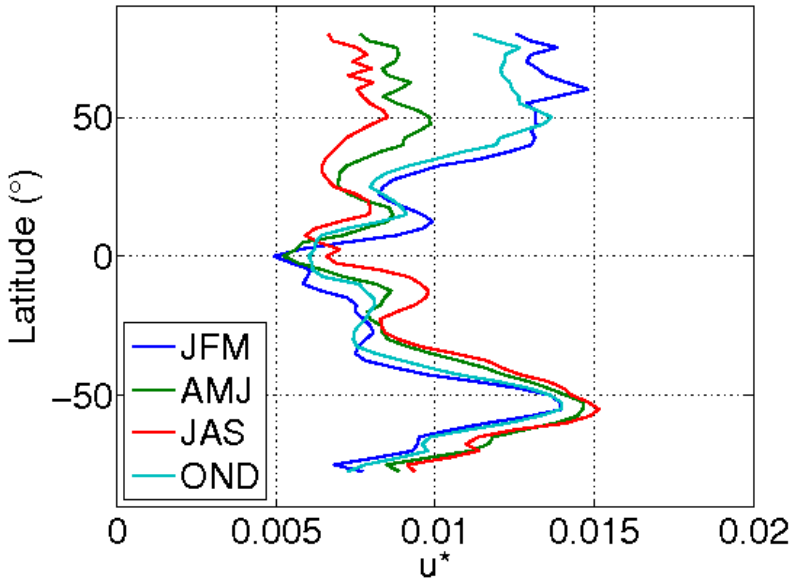

Figure A-9: Seasonal zonal average friction velocity from multimodel ensemble

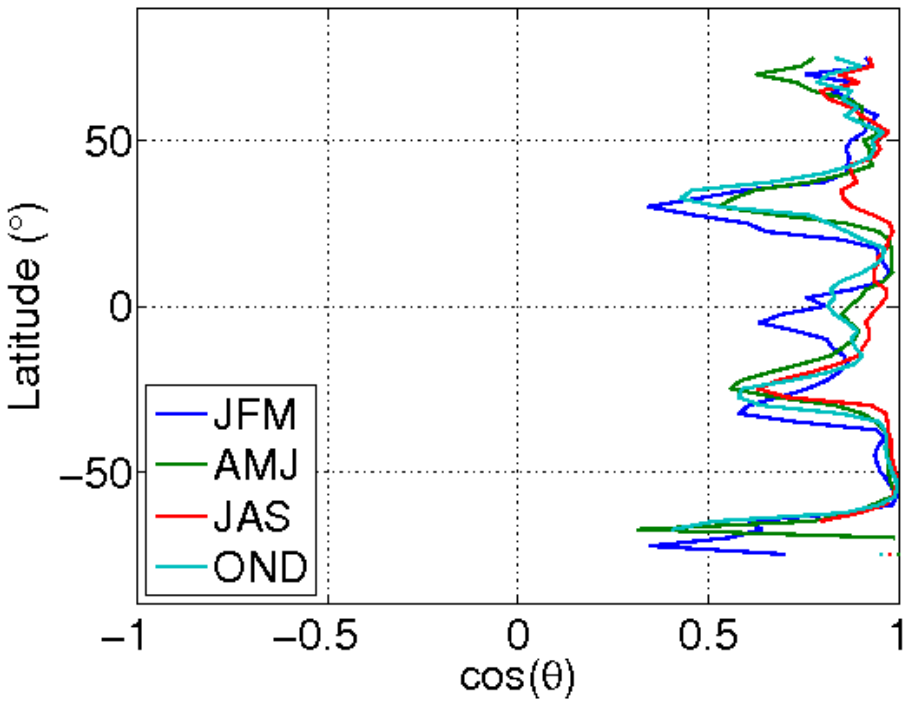

Figure A-10: Seasonal zonal average cos(θ) from multimodel ensemble